INFLUENCE OF ADHESION AT STEEL/MORTAR INTERFACE ON CORROSION CHARACTERISTICS OF REINFORCING STEEL

By
Henrik Axelsson
David Darwin
Carl E. Locke, Jr.

A Report on Research Sponsored by
Department of Civil and Environmental Engineering
University of Kansas

Structural Engineering and Engineering Materials
SL Report 99-4

UNIVERSITY OF KANSAS CENTER FOR RESEARCH, INC.
LAWRENCE, KANSAS
August 1999

INFLUENCE OF ADHESION AT STEEL/MORTAR INTERFACE ON CORROSION CHARACTERISTICS OF REINFORCING STEEL

ABSTRACT

The mechanism of corrosion of reinforcing steel in concrete is discussed based on electrochemical and electron microscopy observations.

The importance of calcium hydroxide precipitation on the steel surface in the steel/mortar interface is evaluated by placing filter paper around reinforcing steel bar specimens prior to casting in mortar, thus preventing direct contact between steel and mortar. The voids created presumably prevent calcium hydroxide crystals from forming on the steel surface. Specimens with filter paper are compared to specimens with good steel/mortar adhesion using rapid macrocell and corrosion potential tests and a scanning electron microscope (SEM) equipped with an energy dispersive spectrometer (EDS). The study included 21 macrocell and 16 corrosion potential tests run for periods of 25 to 89 days. Seven specimens were subjected to SEM/EDS analysis.

Electrochemical results are mixed due to the influence of crevice corrosion, but it is generally shown that better protection is provided for steel with good steel/mortar adhesion than with filter paper. The filter paper, indeed, prevents calcium hydroxide crystals from forming on the steel surface. Corrosion products on active specimens with good mortar cover are shown to grow preferentially in voids created by air bubbles trapped in the mortar. The protective mechanism of calcium hydroxide crystals is proposed to be due to pH buffering by the hydroxyl ions released when the crystals are dissolved, a fact that cannot be proven easily, since many other factors may contribute to the protection of steel in concrete.

ACKNOWLEDGMENTS

This report is based on research by Henrik J. Axelsson in partial fulfillment of the requirements of the M.Sc. degree in Engineering Physics at Chalmers University of Technology, Gothenburg, Sweden. The research was sponsored by the Department of Civil and Environmental Engineering at the University of Kansas and by Structural Metals, Inc.

TABLE OF CONTENTS

LIST OF TABLES

LIST OF FIGURES

LIST OF SPECTRA

CHAPTER 1
INTRODUCTION

1.1 General

The deterioration of reinforced concrete structures due to chloride induced corrosion results in large maintenance and repair costs annually. Chlorides from roadway deicing agents and seawater or salt spray penetrate the concrete and reach the reinforcing steel, causing corrosion of the steel. The chlorides can reach the reinforcement by either diffusing through the porous concrete medium or entering through cracks in the concrete matrix. The corrosion products take up a much larger volume than the original volume of the steel, eventually leading to cracking and spalling of the concrete cover. The cracking and spalling, rather than the dissolution of the reinforcing steel, is usually the key concern associated with the corrosion of steel in concrete.

Concrete normally provides reinforcing steel with an alkaline environment with a pH at the steel surface between 12.6 and 13.8 (Yonezawa, Ashworth and Procter 1988). Under these conditions, the reinforcing steel is protected from corrosion by a passive oxide layer (Broomfield 1997) formed on the steel surface. Penetration of chlorides to the interface, however, leads to localized breakdown of the passive layer and pitting corrosion, with locally lowered pH and a shift in the steel potential.

The purpose of this study is to investigate the nature of the processes taking place in the steel/concrete interface. It has been suggested by Yonezawa et al. (1988) that the formation of $Ca(OH)_2$ crystals on the steel surface works as a buffering factor against the locally decreased pH of pits. This, in turn, lowers the steel's susceptibility to corrode as long as $Ca(OH)_2$ crystals are still present and slowly being dissolved into the solution in the interface. The crystals presumably form on the surface only when the concrete has good adhesion to the steel. Thus, macroscopic voids in the mortar cover would prevent the $Ca(OH)_2$ from forming.

This study, which duplicates parts of the research performed by Yonezawa et al. (1988), involves using filter paper to separate reinforcing steel from adjacent cementitious material, in this case mortar. The goals of this study involve evaluating the

importance of good adhesion between mortar and steel and gaining a broader understanding of the mechanism of corrosion of steel in concrete.

1.2 Corrosion of Steel in Concrete

Concrete is a porous medium allowing chlorides and oxygen to diffuse to the steel/concrete interface. Reinforcing steel is normally passivated in the alkaline concrete environment. The passive layer is maintained and self repaired as long as the environment does not change (Broomfield 1997). The ingress rate of chlorides is increased by the capillary effect (if the concrete is dry before exposing it to the chloride containing solution) and cracks in the concrete, but decreased by larger concrete cover and lower concrete permeability. Chlorides diffusing through the concrete work as catalysts for pitting corrosion when the concentration is high enough to destroy the passive layer. Breakdown of the passive layer shifts the steel potential and a corrosion cell, consisting of an anode and a cathode, is created. The anodic reaction of pitting corrosion takes place in a pit in the material with large surrounding anodes. The pH in the pit decreases rapidly through the hydrolysis reaction (Jones 1996):

$$Fe^{2+} + 2H_2O + 2Cl^- \rightarrow Fe(OH)_2 + 2H^+ + 2Cl^- \qquad (1)$$

The hydrolysis reaction is also valid for crevice corrosion, a variation of pitting corrosion where the steel surface is partly shielded from access of oxygen.

Since chloride attack and the following breakdown of the passive layer changes the steel potential, larger corrosion cells, called macrocells, may be set up. Macrocells occur between steel in uncontaminated environments with electrical connection to attacked steel. The concrete acts as an ionic conductor.

While several different kinds of corrosion products are produced by the combined effects of macrocell and pitting corrosion, it is informative to discuss the formation of hydrated ferric oxide, usually referred to as red rust. The dissolved iron ion combines with the hydroxyl ions in the solution (Broomfield 1997):

$$Fe^{2+} + 2OH^- \rightarrow Fe(OH)_2 \quad \text{(ferrous hydroxide)} \qquad (2)$$

$$4Fe(OH)_2 + O_2 + 2H_2O \rightarrow 4Fe(OH)_3 \quad \text{(ferric hydroxide)} \qquad (3)$$

$$4Fe(OH)_3 \rightarrow Fe_2O_3 \cdot H_2O + H_2O \quad \text{(hydrated ferric oxide)} \qquad (4)$$

As the reactions proceed, tension is created in the surrounding concrete since the hydrated ferric oxide has a volume two to ten times larger than the original steel. As corrosion products accumulate in the interface, the tension eventually reaches a value that causes the concrete to crack.

1.3 Rapid Corrosion Tests

To reduce the time needed to study the corrosion process, rapid corrosion tests have been designed by previous investigators (Martinez, Darwin, McCabe and Locke 1990) at the University of Kansas. These tests are used, with some modifications, in the current study. The test specimens used for the rapid corrosion tests have a fairly thin mortar cover (9.5 mm) to allow rapid chloride ingress. The specimens are cured in lime-saturated water for no more than one week, providing a more porous mortar. After curing, the specimens are allowed to dry for one day. The combined factors result in specimens with low corrosion initiation times.

Two different kinds of tests are used: the macrocell test and the corrosion potential test. The macrocell test is used to measure the corrosion rate of a specimen submerged in simulated concrete pore solution with sodium chloride added. The corrosion rate is determined by measuring the potential drop over a resistor through which the macrocell current is flowing. The voltage drop is transformed to a corrosion rate using Faraday's law (Jones 1996):

$$r = 3.27\frac{aV}{ARnF} \qquad (5)$$

where r is the corrosion rate in micrometers per year, a the atomic weight, V the voltage drop in volts, A the exposed area in cm^2, R the resistance in Ohms, n the number of

equivalents and F Faraday's constant (96500 coloumbs/equivalent). The number of equivalents means the number of electrons exchanged in the chemical reaction.

Corrosion potential test specimens are submerged in simulated pore solution with or without sodium chloride. The potential of the steel is measured with respect to a saturated calomel reference electrode (SCE). The corrosion potential indicates whether the steel surface is active or passive. A potential versus SCE of around –200 mV indicates a passive condition, while a potential of –300 mV or lower indicates an active condition. A passive steel surface is far less likely to corrode than an active one.

In the current study, filter paper is placed around some of the steel specimens prior to casting to prevent direct contact with the mortar. The corrosion performance of these specimens is compared with those without filter paper.

1.4 Objective and Scope

The mechanism of the corrosion of reinforcing steel in concrete is studied using electrochemical measurements and a scanning electron microscope/energy dispersive spectrometer evaluation of the discontinued test specimens. The study involves conventional (black) and stainless steel clad bars cast in mortar, with and without filter paper, and in simulated concrete pore solution with and without sodium chloride. The purpose of the filter paper is to prevent direct contact at the steel/mortar interface while allowing free movement of pore fluid. The electrochemical tests consist of rapid macrocell and corrosion potential tests. The steel/mortar interface is studied using a scanning electron microscope and energy dispersive spectrometer. The study duplicates parts of research by Yonezawa et al. (1988), who investigated and attempted to explain the corrosion mechanism of steel in concrete.

The rapid corrosion tests are performed with simulated pore solution with and without a 1.6 m ion concentration of sodium chloride. A total of 17 macrocell tests and 16 corrosion potential tests are performed. The test period, during which the respective tests were run, varies with the importance and results of the test in question. Test specimens showing interesting or contradictory electrochemical behavior were chosen for the scanning electron microscope and energy dispersive spectrometer evaluation.

CHAPTER 2
EXPERIMENTAL WORK

The experimental work for the rapid corrosion tests and the scanning electron microscope evaluation is presented. The rapid corrosion tests are modified versions of tests developed at the University of Kansas by Martinez, Darwin, McCabe and Locke (1990). Several subsequent researchers have used these tests (e.g. Senecal, Darwin and Locke 1995). Two tests were used in the study – the rapid macrocell and corrosion potential tests. Both tests use simulated concrete pore solution with and without sodium chloride added.

In some test specimens, steel is separated from mortar using filter paper. A description of the fabrication of test specimens and test procedures for the macrocell and corrosion potential test is given. The test specimens were examined using a scanning electron microscope with an energy dispersive x-ray spectrometer after finishing the rapid corrosion tests.

2.1 Materials

The reinforcing steel used for this study was used in a larger study of the corrosion characteristics of reinforcing steel. Two sizes of steel were used – ASTM No. 5 (16 mm diameter) and No. 6 (19 mm diameter) black reinforcing steel bars. Stainless steel (type 304) clad reinforcing steel was also used. The mortar used had a water to cement ratio of 0.5 and a sand to cement ratio of 2. Type I portland cement and ASTM C 778 graded sand were used. Herberts O'Brien™ Nap-Guard® Rebar Patch Kit epoxy was used for patching bare areas needing protection. See Table 2.1 for further details.

2.2 Test Specimens

The No. 5 and No. 6 bar test specimens were 5 in. (127 mm) long. The No. 5 reinforcing bars were used in the macrocell tests only. The specimens were cast symmetrically 3 in. (76 mm) deep in a 4 in. (102 mm) long mortar cylinder with a diameter of 1.5 in. (38 mm). The thickness of the mortar cover was 0.37 in. (9.5 mm) around the specimen (see Figure 2.1). For easy referral, the mortar specimen is denoted a

"lollipop" specimen due to its shape. Some of the macrocell specimens had one piece of filter paper around the steel, while the corrosion potential tests had two pieces of filter paper (see Figure 2.2). Both the molds and the diameter of the reinforcing steel used were modified from the original study by Martinez, Darwin, McCabe and Locke (1990).

2.3 Specimen Fabrication

The reinforcing steel bars were cut to a length of 5 in. (127 mm). One end was drilled and tapped to a depth of 1 in. (2.5 mm) to attach an electrical wire using a 10-24 $^{3}/_{8}$ in. screw (see Figure 2.1). A 0.8 in. (20 mm) wide epoxy band was applied with the centerline 2 in. (51 mm) from the drilled and tapped end to protect the specimen from crevice corrosion were the bar exits the mortar (see Figure 2.1). The best adhesion between steel and epoxy was achieved by sandblasting the metal surface to remove mill scale and residues prior to coating. Tape was used to prevent other parts of the specimen from being accidentally sandblasted in the process. The bottom part of specimens (in mortar) and the electrical connection were also epoxy coated. In some macrocell tests, corrosion products were seen on the exposed portion of the bar (see Figure 2.1), indicating that it might be advisable to epoxy coat the full length of the exposed steel. For this reason, some of the corrosion potential specimens were epoxy coated all the way from the band to the electrical connection. Epoxy coatings were applied in two layers, leaving two hours between coatings and thereafter 24 hours for full cure (at room temperature).

The filter paper specimens were fabricated with standard coarse filter paper cut in 75 mm squares. Double-sided tape was used for adhesion to the bar and to simplify the process of wrapping the filter paper around the specimen. The initial specimens had one piece of filter paper but, after running the macrocell tests for a while, it was concluded that two pieces would be a better choice. One batch of eight specimens with different filter paper configurations was made to check the procedures.

After wrapping and taping one or two pieces of filter paper (each totally covering the specimen with a small overlap), black elastic electrical tape was used to seal the top and bottom of the filter paper. Masking tape was used for the longitudinal seam. Last,

small pieces of masking tape were taped on the bottom on the specimen to fully prevent mortar from reaching the steel surface (see Figure 2.2).

Figure 2.3 shows the mold used to cast specimens. The individual parts designated A through G are described in Table 2.2. All of the materials for the mold were acquired at a local hardware store. Molds are combined to allow simultaneous casting of eight specimens. The molds are assembled as follows: The small rubber stopper (part D) is inserted into the small PVC fitting (part E) (see Figure 2.3). The large rubber stopper (part C), used to keep the specimen centered in the mold, is inserted into the large PVC fitting (part B). The specimen is then inserted upside down into the small PVC fitting (E) through the hole in the small rubber stopper (part D). To avoid the rubber stopper from sliding out of the fitting part, it is pressed against the PVC pipe (part G) supported by a table. The specimen is inserted 2 inches (51 mm) into the rubber stopper, leaving 3 in. (76 mm) to be covered with mortar. The specimen embedded in the small rubber stopper and PVC fitting (parts E and D) are then inserted into the large PVC fitting with the large rubber stopper (parts B and C) to provide stability and center the specimen in the mold. The rubber stopper (part C) is pushed into the PVC fitting (part B) to stabilize the specimen. The longitudinal cut used to remove the completed specimen from the PVC pipe (part G) was taped with masking tape to prevent leakage. The pipe is then inserted into the small PVC fitting (part E). The assembly is placed between wooden boards (part A). Washers and wing nuts are used to tighten down the upper part and stabilize and center the molds between the boards. Before putting the filter paper specimens in the molds, the filter paper was saturated with pre-collected bleed water from mortar later used as filling material around the specimens. The filter paper specimens were then placed in the molds, with care not to damage the filter paper.

The mortar was mixed using the proportions and materials given in Table 2.1. The specimens were cast and cured in an air-conditioned room, since specimens in several batches that were cured in a non-air-conditioned room had voids.

The cement and sand were mixed for approximately one minute before adding the water. After adding water, the mortar was mixed for four minutes in two minute-blocks with manual mixing in between. Manual mixing is needed to prevent unmixed material from sticking to the bottom of the bucket. Immediately after mixing the mortar, it was

poured into the molds on a 60 Hz vibrating table. The mortar was poured in three layers. Between each layer, the specimens were first vibrated for 5 seconds, then rodded 25 times to work the mortar between the mold and the reinforcing bar. The rod was allowed to penetrate into the previous layer to remove voids between the layers. After rodding, each layer was vibrated for four minutes.

The specimens were cured for 24 hours in the molds and then removed from the molds and placed in a curing tank containing lime-saturated water. The first batches of specimens were cured for seven days and the latter batches for three days.

The specimens were removed from the curing tank after seven or three days, and the tapped ends were dried with compressed air. Standard insulated copper wire was used for the electrical connection. The wire was attached to the reinforcing bar with the 10-24 $^3/_8$ in. screw. The screw and the top of the specimen were coated with epoxy so as not to have two dissimilar metals exposed to a corrosive environment. Finally, the specimens were air cured for 24 hours before starting the tests, giving a total curing time of nine or five days for the respective specimens.

2.4 Test Procedures - Macrocell Tests

The macrocell test was designed to measure the corrosion rate. The anode specimens were placed in simulated pore solution with sodium chloride (1.6 molal ion concentration or 4.67%), while the cathode specimens were placed in pure simulated pore solution (see Figure 2.4). This setup simulates the "real world" experience with bridges, where parts of the pore solution in the concrete may be contaminated with salt and other parts may not.

The chemical composition of pore solution is based on an analysis by Fazammehr (1985), who concluded that it contains potassium hydroxide, sodium hydroxide and sodium chloride. Because of the extremely small sodium chloride concentration in pure pore solution (about 0.01%), it was excluded from the pure pore solution expression. Concentrations of pore solution with and without sodium chloride are given in Table 2.3.

A potential difference is established between the specimens as soon as the specimen in a more severe environment loses its passivity. The potential difference drives a current through the 10-ohm resistor connected between the specimens. The same kind of steel

was used for cathode specimens, but without mortar cover. Two cathode specimens were used for each anode specimen so that the cathode would not be the limiting factor in the corrosion behavior. The two cathode specimens were coupled electrically in the container and connected to the resistor.

The solutions were placed in plastic storage containers (see Table 2.4) with lids, and the mortar specimens were submerged 95 mm (3.7 in.) into the solutions. The batch of No. 5 bar specimens without mortar were submerged only 65 mm (2.6 in.), to provide approximately the same length of exposed steel as obtained for the specimens with mortar. The cathodes were also submerged 65 mm (2.6 in.) in the solution. In both cases, the length of the specimen exposed to the solution/mortar was 65 mm (2.6 in.). The specimens without mortar were held upright in the container with a piece of Styrofoam fitting the container and with holes cut in it for the specimens. The electrical wires passed through the lid of the container, to a terminal box where the resistors were mounted for easy recording of the voltage drop. Specimens with mortar were put in the container together with "mortar fill" to better simulate the mortar environment and to support the specimen in an upright position (see Figure 2.4). The mortar fill consisted of mortar pieces that had been cast on baking sheets, cured and then broken into pieces of suitable size to fit around the specimens in the containers. The composition of the mortar fill was the same as for the mortar specimens.

Salt bridges provided an ionic path between the containers. They were constructed by filling flexible plastic tubing with a salt gel consisting of Agar, water and potassium chloride (KCl) (see Table 2.1 for mix proportions). The mix is heated with a Bunsen burner until the gel starts to form, and then rapidly poured into 30 in. (76.2 cm) pieces of tubing. To complete the process, the salt bridges are placed in boiling water for approximately two hours.

Air, scrubbed to remove CO_2, was bubbled through the cathode solutions to provide oxygen. The air scrubber was constructed with a 19-liter (5 gallon) plastic container filled with 1 M NaOH solution. Compressed air was passed through plastic tubing to the bottom of the container and bubbled through the solution by flowing through small holes in the tubing. The air was then tapped off at the top of the container into a system of tubes providing scrubbed air for up to 30 cathode containers. A clamp

on the tubing leading to each cathode container was used to adjust the flow rate. Since the container containing the NaOH was pressurized, the air connections had to be sealed with glue to prevent the air from leaking out.

Readings of the voltage drop over the resistor were taken immediately after the corrosion cell was created. The readings were then taken on a daily basis. Using Faraday's law (see Appendix – Sample Calculations), the voltage drop was converted to a corrosion rate in micrometers per year and plotted as a function of the time in days. The areas used for the corrosion rate calculations were based on the nominal diameters of the bars (16 mm and 19 mm for No.5 and No. 6 bars respectively) and the 65 mm exposed length.

2.5 Macrocell Test Program

The purpose of the macrocell tests was to compare the corrosion rate of reinforcing bar with and without filter paper. No. 5 reinforcing bars were used for a screening test without mortar to determine the corrosion rate of black steel without mortar. The first batches of mortar test specimens were made with one filter paper and without double-sided sticky tape. Three macrocells each containing No. 6 and No. 5 black reinforcing bars and two macrocells with stainless steel clad reinforcing bars were initiated (see Table 2.4). The initial batches of specimens did not include any mortar specimens without filter paper. A review of the filter paper specimen fabrication procedure was performed by breaking off the mortar on specimens from a batch with different filter paper configurations. The conclusion of the review was that two pieces of filter paper are more effective in preventing the mortar from coming in contact with the steel surface. Three more macrocell tests with mortar and filter paper and three with mortar only were started. In all tests, pore solution with sodium chloride for the anode and pure pore solution for the cathode were used.

During the test period, extra salt bridges were added to some macrocell tests. Some test specimens were moved to different containers due to unusual electrochemical behavior.

The test macrocell test specimens are labeled according to Table 2.4, where the first M means macrocell, B means black steel, S means stainless steel, F filter paper (or the

lack thereof), M mortar, and s (lower case) means No. 5 reinforcing bar. Bars not designated s are No. 6 reinforcing bars.

2.6 Test Procedures - Corrosion Potential Tests

In the corrosion potential test, the potential of the steel surface in the test solution is measured. The potential measurements were made with respect to the saturated calomel electrode.

The test setup (Figure 2.5) was similar to that used for the macrocell tests, but with the calomel electrode replacing the cathode, no resistor connecting the electrodes, and maintenance of an open circuit except when the potential was measured. Specimens were cured for three days in lime-saturated water and then one-day in air before submersion. Four specimens of the same kind (e.g., black steel with mortar but without filter paper) were placed in the same container surrounded by mortar fill. Pore solution or pore solution with salt was placed in the containers. Scrubbed air was bubbled into the solutions to provide oxygen. Each specimen was connected to a terminal box with standard insulated copper wire, and a salt bridge connected the test solution with the container with saturated potassium chloride (KCl) in which the calomel reference electrode was submerged. The reference electrode was connected electrically to the specimen via a voltmeter to create a closed circuit. The voltage measurement was recorded on a daily basis and plotted as a function of time of submersion.

2.7 Corrosion Potential Test Program

The corrosion potential tests were used to compare the corrosion characteristics of specimens with or without filter paper.

The filter paper specimens for the corrosion potential test used two pieces of filter paper. A total of 16 specimens in four different configurations were monitored. The tests included black steel with mortar in pore solution and pore solution with sodium chloride (four specimens of each) and black steel with mortar and filter paper in pore solution and pore solution with sodium chloride (four of each). The test configurations are summarized in Table 2.4.

Due to corrosion products on the part of the bar exposed to the vapor phase on black steel bar specimens in the macrocell test, some test specimens were epoxy coated from the epoxy band to the electrical connection.

The corrosion potential test specimens are labeled with P for potential, B for black steel, F for filter paper, and P or S for pore solution or pore solution with sodium chloride (see Table 2.4). No. 6 bars were used for the corrosion potential tests.

2.8 Visual Inspection of Discontinued Tests

As tests were discontinued, the specimens were tagged for identification purposes. A visual inspection of the steel surface, the epoxy coating, and the mortar cover was made. The visual inspection helped explaining some of the discrepancies that appeared in the electrochemical measurements. After evaluating the outside of the specimen, the mortar was cracked of. The mortar pieces were examined for voids, problems with the filter paper cover, crevice corrosion at the bar/epoxy interface and corrosion products in general. The bar surface was examined with a light microscope, providing information for the selection of areas on the specimens to examine further using the scanning electron microscope (SEM) and energy dispersive spectrometer (EDS). A hacksaw was used to cut specimens, first longitudinally and then transversally, to provide reinforcing bar slices sized for SEM and EDS analysis. Additionally, some mortar cover pieces were split into suitable sizes for SEM analysis.

2.9 Scanning Electron Microscope Evaluation

The cut pieces were mounted with conductive double-sided sticky carbon tabs on aluminum stubs. Conductive carbon paint was used to provide a good conductive path from the top of the specimen to the stub. A scanning electron microscope uses a beam of electrons accelerated to energies in the range 0.2-30 keV. Depending on the specimens' ability to conduct the electrons in the beam to ground, the specimens may have to be coated with a thin layer of conductive material to avoid electrons from piling up at the surface (a phenomenon called charging). It was concluded, in screening tests without conductive coating, that coating the specimens with gold-palladium would not interfere with the spectral lines of any of the elements involved, except oxygen. The Mα peak of

palladium will interfere with the Kα peak of oxygen in the low energy region. This constitutes a problem only when the intensity of the oxygen Kα peak is low. The interference problem was avoided automatically, since the materials on the bar surface are oxides, giving strong oxygen peaks. An Anatech Hummer X sputter coater was used to coat the specimens with a 10-20 nm thick layer of gold-palladium. The coating thickness was sufficient to prevent charging, but thin enough to produce minimal interference.

The specimens were examined using secondary electron analysis on a Philips SEM 515 30kV scanning electron microscope. Secondary electron analysis was used to record micrographs of the surface morphology using an ELMDAS digital image acquisition system. An EDAX PV9900 energy dispersive spectrometer was used for compositional analysis. The analyses were made using accelerating voltages of 0.9 kV to 25 kV, with spot sizes ranging from 10 nm to 500 nm.

CHAPTER 3
RESULTS AND DISCUSSION

The electrochemical measurements and scanning electron microscope/energy dispersive spectrometer evaluation of the specimens are presented and discussed in this section.

3.1 Macrocell Tests

The corrosion rates of black No. 5 bars without mortar shown in Figure 3.1 give a good idea of corrosion rates to be expected from black steel without mortar in the particular test setup. These "screening" tests were used to evaluate the test setup and provide data to compare with the mortar test specimens. A peculiarity in the test setup was detected when discontinuing the MBs3 test specimen, which caused the corrosion rates of the two remaining specimens to rise significantly. To investigate the process involved, an additional salt bridge was added to the test setup, resulting in a substantial increase in the corrosion rates. With the extra salt bridge added, the corrosion rates range from 30 to 50 micrometers per year. Visual inspection of the specimens shows crevice corrosion under the bottom epoxy coating. Table 3.1 gives results from the visual inspection of the test specimens.

Figure 3.2 shows corrosion rates for No. 6 reinforcing steel test specimens with one piece of filter paper and mortar. The corrosion rate of the MBFM3 specimen is much higher than for the two others. The visual inspection of the mortar and filter paper revealed cracks in the mortar cover (see Table 3.1), allowing rapid inflow of chlorides. No mortar was found on the steel surface, which was corroded to a large extent. Crevice corrosion was found under the bottom epoxy coat. The MBFM1 and MBFM2 specimens with lower corrosion rates were covered with mortar indicating the specimen fabrication procedure with one piece of filter paper was not working.

The No. 5 bars with one piece of filter paper show varied corrosion behavior (see Figure 3.3). Visual inspection of the specimens reveals mortar coverage ranging from about 40% (MBFMs2) to 90% (MBFMs1). Crevice corrosion was detected under the

bottom epoxy coating (MBFMs2) and under the epoxy band (MBFMs3). Areas close to crevice corrosion show corrosion products.

Using the results from the macrocell tests with one piece of filter paper and without mortar, mean corrosion rates were calculated (see Figure 3.4). The corrosion behavior of the specimens with one filter paper is mixed due to failure of the piece of filter paper to prevent mortar from reaching the steel surface.

Figure 3.5 shows No. 6 black steel bar specimens with mortar and two pieces of filter paper. MBFM4 and MBFM5 show a near constant corrosion rate of 10 micrometers per year after the 20 first days of the test period, while the corrosion rate of MBFM6 changes. The MBFM6 specimen was moved to a new container since it was believed that the other specimens influenced the corrosion behavior. After moving the specimen to an independent solution on day 43, the corrosion rate increased to about 10 micrometers per year, while the corrosion rate of the two other specimens remained unchanged. Visual inspection showed that two pieces of filter paper effectively block adhesion between mortar and steel. When the mortar cover was removed, the filter paper was moist and the steel surface covered with a liquid film. The bottom epoxy coating showed crevice corrosion, but corrosion products were found all over the surface.

Corrosion rates for specimens without filter paper are shown in Figure 3.6. One specimen (MBM3) had a damaged mortar cover with large amounts of corrosion products in a crack in the epoxy band. The other specimens show nearly constant corrosion rates, with an average rate between 2 and 2.5 micrometers per year. Visual inspection of the specimens shows small amounts of corrosion products preferentially developed in the inevitable voids present in the mortar cover. The voids in mortar specimens with good mortar adhesion may be formed due to air bubbles trapped at the steel/mortar interface when casting the specimens. The transverse ribs on the reinforcing steel may constitute one source of void formation, as air bubbles may be trapped. No visible crevice corrosion was found on the mortar specimens without filter paper.

The mean corrosion rates for the black steel specimens with two pieces of filter paper and without filter paper are shown in Figure 3.7. It is clear that specimens with filter paper have higher corrosion rates.

Figure 3.8 shows the results for the stainless steel clad reinforcing steel. Corrosion rates range from 0 to 0.5 micrometers per year. Due to the very low corrosion rates, no corrosion products were seen on the steel surface when removing the mortar cover. More than half of the specimen surface showed good adhesion of the mortar cover, but some parts were totally uncovered without signs of cementitious material.

3.2 Corrosion Potential tests

The results from the corrosion potential tests show that specimens with filter paper are more active (i.e. have more negative corrosion potentials) than the corresponding specimens without filter paper. Two test specimens without filter paper were epoxy coated on the air-exposed part of the bar to evaluate the influence of corrosion in the vapor phase of the test container.

Figure 3.9 shows the corrosion potential for specimens with mortar and without filter paper in pure pore solution. Three of the specimens passivate at a potential around –200 mV versus SCE and one (PBP2) is active with a potential growing progressively more negative with time. The entire air-exposed piece of PBP2 was epoxy coated. The same shape of the corrosion potential graph versus time can be seen for the epoxy coated PBS3 specimen (see Figure 3.10). These measurements strongly suggest that epoxy coating the whole piece was a poor decision. The other mortar specimens without filter paper in pore solution with sodium chloride behave as expected from earlier similar tests, with corrosion potentials ranging from –350 mV to below –600 mV some time after submersion.

The behavior of the filter paper specimens in pure pore solution is unexpected. Reinforcing steel normally passivates in simulated pore solution, but the corrosion potentials range from –350 mV to below –500 mV after 20 days (see Figure 3.11). Removing the mortar cover on the PBFP2 specimen showed crevice corrosion under the epoxy band, which may explain the strange behavior.

Corrosion potentials for the filter paper specimens in pore solution with sodium chloride show the largest activity among the test specimen groups (see Figure 3.12). The corrosion potentials range in a narrow band between –500 mV and –600 mV. Crevice corrosion under the epoxy coating of specimens makes it difficult to draw conclusions,

since the crevice corrosion rather than other processes may have created the lower potentials of the filter paper specimens.

A summary of the corrosion potential test potentials is given as mean corrosion potentials for the respective specimen groups in Figure 3.13, excluding specimens PBP2 and PBS3. Mortar specimens without filter paper are generally more passive than filter paper specimens. At 29 days, though, the mean corrosion potential of mortar specimens in pore solution with sodium chloride is nearly as negative as for specimens with mortar and filter paper in pore solution with sodium chloride (see Figure 3.13).

3.3 Scanning Electron Microscope Evaluation

It was proposed by Yonezawa et al. (1988) that $Ca(OH)_2$ crystals would form only on specimens with good adhesion between steel and mortar and that the crystals would dissolve on corroding specimens. The crystals would dissolve because of decreased pH on the steel surface due to pit formation on the surface. The dissolution process would act as a pH-buffering factor and slow the rate of pitting corrosion. $Ca(OH)_2$ crystals would not form on steel surfaces with poor adhesion to the mortar.

Combining the two parameters, adhesion and corrosion rates, yields four specimen groups: non-corroding with good adhesion (1), non-corroding with poor adhesion (2), corroding with good adhesion (3) and corroding with poor adhesion (4). Specimens from each group are analyzed with respect of $Ca(OH)_2$ and corrosion products. For the analysis of the first specimen group, a filter paper specimen with broken filter paper and thus good mortar adhesion was used. The results are summarized in Table 3.2.

Figure 3.14 shows what is believed to be $Ca(OH)_2$ crystals on the steel surface of a non-corroded specimen with good mortar adhesion. EDS analysis shows strong peaks for Ca and O and a small peak for Si supporting the assumption (see Spectrum 3.1). EDS analysis does not allow for quantitative analysis of unpolished surfaces, which means that only qualitative information can be retrieved about objects seen on the specimens. This means that the morphology of $Ca(OH)_2$, large plate like crystals, must also be used to identify the material. Such a morphology is supported by the micrograph.

The stainless steel specimens resemble non-corroded specimens with poor mortar adhesion. Parts of the unprotected stainless steel surface show no corrosion products and

no cementitious material. Where the mortar has penetrated the filter paper, cementitious material is detected.

Sparsely distributed $Ca(OH)_2$ crystals can be seen on the surface of corroded specimens with good adhesion (Figure 3.2). EDS analysis (Spectrum 3.2) shows peaks for Ca and O. Corrosion products are observed to grow preferentially in voids in the mortar cover on specimens with good mortar adhesion (Figure 3.16). No $Ca(OH)_2$ was found close to or in the voids where the corrosion products had grown. The corrosion products appear in many different shapes (see Figure 3.17). Spectrum 3.3 shows strong peaks for Fe, Ca and O and smaller peaks for Si, K and Mn. It is inevitable that material from the cement will interfere with the spectrum as pore solution has been present in most cases. It is also possible that the energetic electrons in the electron beam of the microscope pass through the corrosion products and strike the material behind. Mn is part of the mild steel composition.

Corroding specimens with large voids in the mortar cover (group 4) develop corrosion products that grow in large "pipes". The pipes can grow to sub-millimeter or millimeter sizes, easily visible with the bare eye. Figure 3.18 shows a typical corrosion product pipe (seen from above) on the surface of specimen MBFM5. Spectrum 3.4 of the corrosion products shows strong peaks for Fe, Cl and O, suggesting either iron oxide with chlorides deposited on its surface or $FeCl_2$ crystals. Figure 3.19 illustrates the size to which the corrosion products grow and the vast range of different morphologies they show.

Figure 3.20 shows $Ca(OH)_2$ and products from cement hydration found in an area separated approximately 15 mm from the corrosion products in Figure 3.19. Spectrum 3.5 shows strong peaks for Ca and O.

Calcium hydroxide crystals deposited on the inner surface of the inner filter paper (MBFM5 specimen) are shown in Figure 3.21. Crystals are found in few locations on the inner filter paper but in large amounts on the inside of the outer filter paper (Figure 3.22), where the crystals also grow to substantially larger size. Spectra 3.6 and 3.7 show large peaks for Ca and O, while Spectrum 3.6 shows small peaks for Na, Si and K. No chlorides are found in the spectra.

Figure 3.23 shows a specimen with partly good mortar adhesion. An area with poor adhesion shows corrosion products. Next to the void, an area with good mortar adhesion is shown (zoom in, Figure 3.24); calcium hydroxide crystals are deposited on the surface (Spectrum 3.8).

3.4 Influence of Crevice Corrosion

It is difficult to assess to what extent crevice corrosion contributes to the electrochemical results presented. It is known that crevice corrosion shifts the potential of the steel surface, which may explain the active corrosion potential of filter paper specimens in pore solution (Figure 3.11). It can thus be concluded that the reliability of the corrosion potential tests may be questioned. The corrosion potential tests, however, show that the creation of voids in the mortar cover provides a severe environment for the reinforcing steel. Many of the test specimens have elevated amounts of corrosion products on the bare steel surface close to the area of crevice corrosion, indicating that crevice corrosion may affect the microstructure and microchemistry of the surrounding steel surface. Several macrocell specimens, on the other hand, have corrosion products evenly distributed on the exposed surface despite the presence of crevice corrosion under the epoxy coating.

Results from the corrosion potential tests in pore solution with sodium chloride show that the mean corrosion potential of specimens with and without filter paper reaches about the same value after 29 days (Figure 3.13). The corresponding comparison for the macrocell tests, though, shows that the mean corrosion rates for specimens with two pieces of filter paper are at least three times larger than for mortar specimens without filter paper (Figure 3.7). This implies that the higher mean macrocell corrosion rates cannot be explained by crevice corrosion only. There is no evidence that crevice corrosion interferes with the results to the extent that the measurements are unreliable, but it must be taken into account.

3.5 Mechanism of Corrosion of Steel in Concrete

The protection that is provided for reinforcing steel in concrete is a subject not fully understood. It has been proposed (Yonezawa et al. 1988) that calcium hydroxide crystals formed on the steel surface act as a buffering factor against the lowered pH in corrosion

pits. Furthermore, $Ca(OH)_2$ crystals would not form on the steel surface at large voids in the mortar cover where no direct contact exists between the steel and the mortar.

Page and Treadaway (1982) gave another explanation for the protection of steel in concrete. They suggested that a lime-rich layer on the steel surface would limit the oxygen access to the surface and thus reduce the cathode reaction rate in pitting corrosion. Leek and Poole (1990) ascribe the protective mechanism for the steel to a two-component system consisting of an inner passive oxide layer and an outer layer of calcium hydroxide with inclusions of calcium-silicate-hydrate gel. The main protection would come from the passive oxide layer.

The SEM/EDS evaluation neither confirms nor rejects the results by Yonezawa et al. (1988). This study shows that good adhesion between mortar and steel gives better protection against corrosion than the environment created in macroscopic voids at the steel/mortar interface. Neither corroded nor non-corroded specimens with filter paper placed in the interface show signs of $Ca(OH)_2$ crystals on the steel surface. $Ca(OH)_2$ is formed on the steel only in areas where mortar/cementitious material has leaked through the filter paper during the casting process. Specimens or areas of specimens with good mortar adhesion, on the other hand show scattered $Ca(OH)_2$ crystals on the steel surface.

It is shown that large amounts of calcium hydroxide form on the inner face of the outer filter paper, suggesting that the growth of $Ca(OH)_2$ is favored in the void created between the filter papers. It is known (Taylor 1997) that $Ca(OH)_2$ crystals tend to grow in originally water-filled spaces between cement grains in young cement paste. The volume created between the pieces of filter paper is characterized by large amounts of cement bleed water (partly due to the saturation of the filter paper prior to casting), with small amounts of cement paste that has leaked through the bulk of the filter paper. Furthermore, this implies that $Ca(OH)_2$ crystals would grow in any water-filled space on the steel surface of specimens with good mortar adhesion.

No calcium hydroxide was found in areas where the steel was corroded, suggesting that either the $Ca(OH)_2$ was dissolved totally or it was not formed in those areas. Also, if calcium hydroxide had not formed, the area would presumably be a favored location for corrosion initiation.

For calcium hydroxide to buffer the pH and decrease the rate of pitting corrosion, the crystals have to be close to the pits. The surface has to be covered with a medium (liquid) in which the $Ca(OH)_2$ can be dissolved and transported to the pit by diffusion. As a void is formed in the mortar cover, the distance between the mortar and the steel may be large enough for the diffusion process to be ineffective. Also, in corroding specimens with good mortar cover, the calcium hydroxide would eventually be consumed by the pits, leading to a state where protection due to calcium hydroxide would be lost.

The SEM examination clearly shows that corrosion products on mortar specimens with good adhesion grow preferentially in macroscopic voids in the mortar cover. The voids may be created by air bubbles trapped in the steel/mortar interface. No calcium hydroxide is found, but debris of cementitious material is deposited in scattered locations in the voids. The absence of calcium hydroxide supports the suggestion that these voids are air-filled thus preventing crystal formation, at least during the relatively short duration of the tests.

The corrosion products show many different shapes and sizes. On specimens with filter paper, the corrosion products show large pipe-like shapes presumably formed on top of pits. The corrosion products formed on the inside of the "pipes" consist of iron, oxygen and substantial amounts of chlorine, supporting the suggestion that the complexes are formed on top of pits with elevated chloride concentrations. The pipes are only formed in large voids in the mortar cover.

The better protection provided by mortar with good adhesion may also be explained by the limited mobility of chloride ions on a surface with good mortar adhesion. It has been shown (Mankowski and Szklarska-Smialowska 1975) that the concentration of chlorides in the pit grows with time in the earlier stages of pit growth and chlorides must thus be supplied. The diffusion of chlorides into homogenous mortar is uniform. Since pits are localized phenomena, the chlorides must be collected from surrounding areas. Tightly adhering mortar would decrease the mobility of chlorides on the steel surface, thus presumably decreasing the rate of pit growth.

The corrosion protection of steel in concrete is likely to be explained by a combination of the mechanisms discussed above. The formation of large voids in the mortar cover weakens the mechanism of protection.

CHAPTER 4
SUMMARY AND CONCLUSIONS

4.1 Summary

Aspects of the mechanism of corrosion of steel in concrete have been evaluated. This study addresses a theory proposed by Yonezawa et al. (1988) suggesting that precipitation of calcium hydroxide on the steel surface in the steel/mortar interface would act as a protective mechanism. Calcium hydroxide crystals, presumably, would not form in voids in the mortar cover where adhesion between the steel and mortar would be blocked. Thus, the protective mechanism would not work in areas with voids. The theory is evaluated by placing filter paper around part of 127 mm (5 in.) long steel bars before casting in mortar, blocking direct adhesion between mortar and steel. Specimens with filter paper were compared with mortar specimens with good adhesion between the steel and mortar. Two different types of reinforcing steel were used for the study, conventional (black) steel and stainless steel clad bars.

Test specimens were tested electrochemically by means of rapid macrocell and corrosion potential tests developed at the University of Kansas. The rapid macrocell test measures the corrosion rate of specimens, while the rapid corrosion potential test measures the potential of the steel surface versus a saturated calomel electrode. After discontinuing the electrochemical tests, the steel/mortar interface was examined using a scanning electron microscope with an energy dispersive spectrometer.

Test specimens with filter paper are very susceptible to crevice corrosion in certain areas, which affects some of the electrochemical results to a large extent. It is not known whether the crevice corrosion put all of the electrochemical measurements at risk.

The mean corrosion rate in the macrocell tests for specimens with filter paper is approximately three times larger than for those with good adhesion. Results from the corrosion potential tests are mixed. The scanning electron microscope evaluation shows that corrosion products grow preferentially in voids in the mortar cover on specimens with good mortar adhesion. Calcium hydroxide is formed in locations with good adhesion, but is absent in voids.

4.2 Conclusions

Conclusions are based on test results and scanning electron microscope/energy dispersive spectrometer evaluation.

1. For mortar to give reinforcing steel full protection against corrosion, adhesion between steel and mortar must be tight.

2. Active corrosion on mortar specimens with good adhesion appears to be located only in voids at the steel/mortar interface. The voids appear to be formed by air bubbles trapped in the mortar when casting the specimens.

3. Calcium hydroxide crystals are not detected on corroding parts of the steel electrodes, implying either the crystals or some other aspect of good mortar cover provides the protective mechanism. It is likely that the mechanism of protection is a combination of several factors, with calcium hydroxide playing a role.

4. $Ca(OH)_2$ crystals do not form on the steel surface in air-filled voids in the mortar cover, at least not for periods up to 89 days.

5. Crevice corrosion alters the results of the rapid corrosion potential and possibly also macrocell tests.

4.3 Future Work

To further investigate the mechanism of corrosion of steel in concrete, the rapid macrocell and corrosion potential tests must be modified to solve the problem with crevice corrosion. Specimen fabrication procedures are likely to be the source of the problems.

Test specimens could be submerged in simulated pore solution, pore solution with salt, and saturated calcium hydroxide, measuring the potential of the steel. Measurements of the polarization resistance could be performed as well as macrocell corrosion rate measurements. The rapid macrocell tests should use one anode-specimen per container only to prevent interference between specimens.

To fully investigate the processes in the steel/mortar interface, the method of scanning electron microscope specimen preparation should be improved and extended to include polished transverse cross sections for quantitative energy dispersive spectrometer analysis and backscatter electron analysis. By cutting very thin slices of cross sections,

electron diffraction methods can be used (Glasser and Sagoe-Crentsil 1989) to determine the phase composition of the (passive) oxide layer and the corrosion products and to detect calcium hydroxide and other products of cement hydration. Other possibilities for determination of corrosion products and hydration products are x-ray powder diffraction and infrared spectroscopy.

REFERENCES

Broomfield, J. P. (1997). *Corrosion of Steel in Concrete – Understanding, Investigation and Repair.*, E & FN Spon, London, 240 pp.

Constantinou, A. G. and Scrivener, K. L. (1995). "The Corrosion of Steel Reinforcement in Carbonated Concrete Under Different Humidity Regimes," *Microstructure of Cement-Based Systems/Bonding and Interfaces in Cementitious Materials: Symposia Held November 28-December 1, 1994, Boston, Massachusetts*, Materials Research Society Symposium Proceedings, Vol. 370, pp. 471-478.

Foley, R. T. (1970). "Role of the Chloride Ion in Iron Corrosion," *Corrosion*, Vol. 26, No. 2, pp. 58-70.

Glasser, F. P. and Sagoe-Crentsil, K. K. (1989). "Steel in Concrete: Part II – Electron Microscopy Analysis," *Magazine of Concrete Research*, vol. 41, No. 149, Dec., pp. 213-220.

Glasser, F. P. and Sagoe-Crentsil, K. K. (1993). "Constitution of Green Rust and Its Significance to the Corrosion of Steel in Portland Cement," *Corrosion*, Vol. 49, No. 6, pp. 457-463.

Goldstein, J. I., Newbury, D. E., Echlin, P., Joy, D. C., Romig, A. D. Jr., Lyman, C. E., Fiori, C., and Lifshin, E (1992). *Scanning Electron Microscopy and X-ray Microanalysis.*, Plenum Press, New York, 820 pp.

Jones, D. A. (1996). *Principles and Prevention of Corrosion.*, Prentice-Hall, Upper Saddle River, 572 pp.

Mindess, S. and Young, J.F. (1981). *Concrete*, Prentice-Hall, Englewood Cliffs, 671 pp.

Kitowski, C. J. and Wheat, H. G. (1997). "Effect of Chlorides on Reinforcing Steel Exposed to Simulated Concrete Solutions," *Corrosion*, Vol. 53, No. 3, March, pp. 216-226.

Leek, D. S. and Poole, A. B. (1990). "The Breakdown of the Passive Film on High-Yield Mild Steel by Chloride Ions," *3rd International Symposium on Corrosion of Reinforcement in Concrete*, Elsevier Applied Science Publishers, London, pp. 65-73.

Macias, A. and Andrade, C. (1987). "Corrosion of Galvanized Steel Reinforcements in Alkaline Solutions. Part 2: SEM Study and Identification of Corrosion Products," *British Corrosion Journal*, vol. 22, No. 2, pp. 119-129.

Mankowski, J. and Szklarska-Smialowska, Z. (1975). "Studies on Accumulation of Chloride Ions in Pits Growing During Anodic Polarization," *Corrosion Science*, Vol. 15, No.8, Sep., pp. 493-501.

Martinez, S. L., Darwin, D., McCabe, S. L., and Locke, C. E. Jr. (1990). "Rapid Test for Corrosion Effects of Deicing Chemicals in Reinforced Concrete," *SL Report* 90-4, University of Kansas Center of Research, Lawrence, Kansas, Aug., 61 pp.

Mejlhede Jensen, O., Coats, A. M., and Glasser, F. P. (1996). " Chloride Ingress Profiles Measured by Electron Probe Micro Analysis," *Cement and Concrete Research*, Vol. 26, No. 11, pp. 1695-1705.

Page, C. L., and Treadway, K. W. J. (1982). "Aspects of the Electrochemistry of Steel in Concrete," *Nature*, Vol. 297, No. 5862, May, pp. 109-115.

Schwensen, S. M., Darwin, D., and Locke, C. E. Jr. (1995). "Rapid Evaluation of Corrosion-Resistant Concrete Reinforcing Steel in the Presence of Deicers," *SL Report* 95-6, University of Kansas Center of Research, Lawrence, Kansas, July, 90 pp.

Senecal, M. R., Darwin, D., and Locke, C. E. Jr. (1995). "Evaluation of Corrosion-Resistant Steel Reinforcing Bars," *SM Report* No. 40, University of Kansas Center of Research, Lawrence, Kansas, July, 142 pp.

Taylor, H. F. W. (1997). *Cement Chemistry*, 2nd Ed., Thomas Telford Publishing, London, 459 pp.

Weyers, R. E., Pyc, W., and Sprinkel, M. M. (1998). "Estimating the Service Life of Epoxy-Coated Reinforcing Steel," *ACI Materials Journal*, Vol. 95, No. 5 Sep. - Oct., pp. 546-557.

Yonezawa, T., Ashworth, V., and Procter, R. P. M. (1988). "Pore Solution Composition and Chloride Effects on the Corrosion of Steel in Concrete," *Corrosion*, Vol. 44, No. 7, July, pp. 489-499.

Zayed, A. M. and Slater-Haase, A (1992). "The Nature of the Concrete-Steel Rebar Interface and its Effects on Corrosion Initiation," *Paper No. 209 presented at CORROSION/92 NACE Conference*, 10 pp.

Table 2.1 Equipment and materials used in the rapid corrosion tests

Item	Description
Voltmeter	Hewlett-Packard HP3456A Digital Voltmeter
Air scrubber	19 liter (5 gallon) plastic container with 1M NaOH filled to 75 %
Tubing for salt bridges and scrubbed air	Fischer Scientific Flexible Clear Plastic Tubing, inner diameter ¼ in. (6.4 mm), outer diameter $^{3}/_{8}$ in. (9.5 mm) and wall thickness $^{1}/_{16}$ in. (1.6 mm)
Cement for mortar mix	Lonestar Portland Cement Type I
Sand for mortar mix	Unimin Corp. ASTM C 778 graded sand
Mortar mix composition	333g deionized water, 667g Portland cement and 1333g sand (ratios - 1:2:4). These quantities were used casting 8 specimens
Calomel electrode	Fischer Scientific Standard Pre-filled Calomel Reference Electrode with Pin in saturated KCl solution
Protecting epoxy	Herberts O'Brien™ 7-1870 Nap-Guard® Rebar Patch Kit
Salt bridges – mix proportions	4.5g Agar (Sigma High gel Strength Agar), 30g KCl (Fischer Scientific) and 100g deionized water. Filled in 30" pieces of flexible tubing
Scale for weighing of chemicals	Denver Instruments TR4102 Digital Scale
Plastic containers	Consolidated® Plastics Company Inc. 7x7½" (178 x 191 mm, diameter x height), 4.5 l plastic container with lid
Filter paper	Fisherbrand® P8 Coarse Filterpaper (205 mm diameter discs)

Table 2.2 Description of mold assembly used to cast specimens for the rapid corrosion tests (see Figure 2.3)

Part	Description
A	Two pieces of wood with the dimensions 38 mm (1.5 in.) x 140 mm (5.5 in.) x 400 mm (15.7 in.)
B	1.5 in. to 1.5 in. PVC I fitting (ASTM D 2466) with inner diameter of 49 mm (1.93 in.). The total length of the fitting is 69 mm (2.72 in.). A stopping edge with an inner diameter of 45 mm (1.77 in.) is located in the middle of the fitting
C	No. 10 Rubber Stopper with a 19 mm (0.75 in.) centered hole (drilled). The outer diameter of the rubber stopper is 50 mm (1.97 in.) to give a good seal to the PVC fitting (part B)
D	No. 8½ Rubber Stopper with an outer diameter of 43 mm (1.69 in.) and a 19 mm (0.75 in.) centered hole (drilled)
E	1.25 in. to 1.25 in. PVC I fitting (ASTM D 2466) with 42 mm (1.65 in.) inner diameter. The total length of the fitting is 65 mm (2.56 in.). At one end the external diameter is machined down from 50 mm (1.97 in.) to 48 mm (1.89 in.) to allow the fitting to fit with part B. The length of the machined part of the fitting is 36 mm (1.42 in.)
F	Epoxy coated bands on the specimen (placed up side down in the mold)
G	102 mm (4 in.), longitudinally cut PVC pipe (ASTM D 2466) with 38 mm (1.5 in.) inner diameter
H	Six threaded rods with one washer and wing nut on each

Table 2.3 Simulated pore solution with and without sodium chloride. Concentrations with respect to weight of water

Solution	KOH concentration %	NaOH concentration %	NaCl conc. % (molal ion concentration)
Pore solution	1.93	1.83	0 (0 m)
Salt solution (pore solution + NaCl)	1.93	1.83	4.67 (1.6 m)

Table 2.4 Specimens for rapid corrosion tests. p.s. denotes pure pore solution and s.s stainless steel clad bars. All tests, except MSFM1 and MSFM2, used black reinforcing steel

Specimen	# of spec.	Filter paper	Test type	Specimen ID code
No. 5 bar w/o mortar	3	No	Macrocell	MBs1 – 3
No. 5 bar with mortar	3	1 piece	Macrocell	MBFMs1 – 3
No. 6 bar with mortar	3	1 piece	Macrocell	MBFM1 – 3
No. 6 bar with mortar	3	2 pieces	Macrocell	MBFM4 – 6
No. 6 bar with mortar	3	No	Macrocell	MBM1 – 4
No. 6 s.s bar with mortar	2	1 piece	Macrocell	MSFM1-2
No. 6 bar with mortar	4	2 pieces	Corr. pot. pore solution	PBFP1 – 4
No. 6 bar with mortar	4	No	Corr. pot. pore solution	PBP1 – 4
No. 6 bar with mortar	4	2 pieces	Corr. pot. p.s. with NaCl	PBFS1 – 4
No. 6 bar with mortar	4	No	Corr. pot. p.s. with NaCl	PBS1 – 4

Table 3.1 Results from exterior and interior visual inspection of test specimens

Specimen	Description
MBs1 - MBs3	Large amounts of corrosion products on part of bar exposed to air. General corrosion on part in solution. Crevice corrosion under epoxy coating at bottom of specimen
MBFM1	Exterior: No visual cracks in mortar cover and no corrosion products on exposed part of bar Interior: Filter paper was dry when mortar was removed. Single filter paper has provided poor protection against mortar penetration; approximately 90 – 95% of the area has good adhesion with the mortar cover. Very few corrosion products on steel surface. No crevice corrosion
MBFM2	Exterior: No cracks or voids in mortar cover. No corrosion products on air-exposed part of bar Interior: Filter paper was moist when removing mortar cover. Mortar has penetrated filter paper and covers 40% of the steel surface. Crevice corrosion under bottom epoxy coating and corrosion products in a few uncovered locations
MBFM3	Exterior: Two cracks in mortar cover located on opposite sides of specimen. Small amounts of corrosion products on exposed part of bar Interior: Filter paper and steel surface wet when opening mortar cover. The corrosion products seen on steel surface change color from black/green to red/orange in a few minutes. Cracks in mortar cover extend to the bar. Filter paper mostly intact giving poor adhesion between mortar and steel. About 10% covered with mortar. Large amounts of corrosion products due to general corrosion cover the surface of the steel. Some crevice corrosion under epoxy coat at the bottom of specimen. Parts with good mortar adhesion show no corrosion products

Table 3.1 (continued)

MBFMs1	Exterior: Large amounts of corrosion products on air-exposed part of bar. No cracks in mortar cover Interior: Filter paper dry when removing mortar cover. Due to failure of filter paper, approximately 90% of steel surface has good adhesion to mortar. Very small amounts of corrosion products on steel surface. Corrosion products have grown in voids. No crevice corrosion
MBFMs2	Exterior: Small amounts of corrosion products on exposed part of bar. No cracks in mortar cover Interior: Filter paper dry when removing mortar cover. Steel surface partly protected from mortar by the filter paper; approximately 40% area with good adhesion. Moderate amounts of corrosion products are localized on one side of the specimen (poor adhesion), in a 20 mm long band originating in a small area, with crevice corrosion between steel and bottom epoxy layer
MBFMs3	Exterior: Very large amounts of corrosion products on air-exposed part of bar. No cracks in mortar cover Interior: Filter paper was dry when opening specimen. Due to filter paper failure, about 60% of the steel surface has good mortar adhesion. Corrosion products are localized to an area around the epoxy band, where crevice corrosion has taken place. The area of corrosion products extends about 15 mm towards the region exposed to pore solution and salt.
MBFM4	Exterior: No cracks and no corrosion products on exposed part of the bar Interior: Filter paper was moist/wet. Steel surface partly covered with liquid film. Filter paper has totally sealed the steel surface from mortar. Some cementitious material has penetrated through filter paper and been deposited on surface. Solution has penetrated under epoxy coating at bottom part of bar, but a very small amount of corrosion products is seen. General corrosion products in fair amounts are seen over the surface of the bar. This specimen shows more corrosion products than MBFM5

Table 3.1 (continued)

MBFM5	Exterior: No cracks or voids in mortar cover. Some corrosion products on exposed part of bar Interior: Filter paper and parts of steel surface were wet. Small amounts of crevice corrosion under bottom epoxy coating. The epoxy breaks off, easily revealing liquid and corrosion products underneath. General corrosion products spread uniformly on one side of the rest of the specimen. The other side has small amounts of corrosion products
MBFM6	Exterior: No visible cracks or voids in mortar cover. Some corrosion products on air-exposed part of bar Interior: Filter paper and parts of steel surface wet. Some crevice corrosion under epoxy band. Some general corrosion products (less than MBFM4 and MBFM5) in distinct locations uniformly spread out on the surface. Fair amounts of corrosion products in area surrounding the crevice corrosion
MBM1	Exterior: Some corrosion products on air-exposed part of bar. Mortar cover without voids or cracks Interior: No crevice corrosion. Very small amounts of corrosion products on steel surface, preferentially grown in a few voids in mortar cover (formed by air bubbles in the steel/mortar interface). Mortar cover had good adhesion
MBM2	Exterior: Fair amounts of corrosion products on air-exposed part of bar. Mortar cover without voids or cracks Interior: More corrosion products than MBM1 and MBM3 in voids in mortar cover. No visible crevice corrosion under epoxy coatings
MBM3	Exterior: Large amounts of corrosion products on air-exposed part of bar, preferentially close to epoxy band. The mortar cover was damaged; a large chip broken out of mortar cover, leaving parts of the epoxy band bare. The void created was not large enough to expose the steel in mortar. Large amounts of corrosion products have penetrated the epoxy band, suggesting crevice corrosion from underneath and contact with the solution Interior: Very small amounts of corrosion products formed in voids in the mortar cover

Table 3.1 (continued)

MSFM1	Exterior: Mortar cover lacks voids or cracks. No corrosion products on air exposed part of bar Interior: No corrosion products on steel surface. Mortar with good adhesion covers about 60% of steel surface. Some areas of the steel area are totally clean from cementitious material
MSFM2	Exterior: No cracks or voids in mortar cover. Small amounts of corrosion products on top of air-exposed part of the specimen Interior: Approximately 50% of steel surface covered with mortar with good adhesion. No corrosion products
PBFP2	Exterior: No corrosion products on part of bar exposed to air. Mortar cover is homogenous without cracks or voids Interior: Filter paper wet when removing mortar cover. Some of the liquid in the mortar has penetrated and deposited some cementitious material on the surface. Both inner and outer pieces of filter paper have crystals deposited on surface. Some corrosion products formed on surface in different locations. Crevice corrosion under epoxy band showing small amounts of corrosion products
PBFS2	Exterior: Some corrosion products on air-exposed part of bar. No cracks or voids in mortar cover Interior: No adhesion between mortar and steel. No deposits on surface. Filter paper and lower parts of surface were wet when the mortar cover was removed. . Both inner and outer pieces of filter paper have crystals deposited on surface. Corrosion products on scattered locations of specimen. Crevice corrosion under epoxy band

Table 3.2 Scanning electron microscope specimens analyzed. Group number is indicated. MBFMs1 is placed in two groups since parts of the specimen are uncorroded with good adhesion and other parts have corrosion products formed in voids

Specimen ID	Group	Results
MBFM1 (MBFMs1)	Non-corroding, good adhesion (1)	$Ca(OH)_2$ crystals scattered on steel surface
MSFM1	Non-corroding, poor adhesion (2)	No $Ca(OH)_2$ or products of cement hydration in areas with poor adhesion
MBM3 MBM2 (MBFMs1)	Corroding, good adhesion (3)	Very few $Ca(OH)_2$ crystals. Corrosion products formed in voids in mortar cover
MBFM5 MBFM3	Corroding, poor adhesion (4)	Corrosion products grown on arbitrary part of steel surface in large complex structures. $Ca(OH)_2$ and products of cement hydration on some uncorroded parts of surface associated with leaks in the filter paper

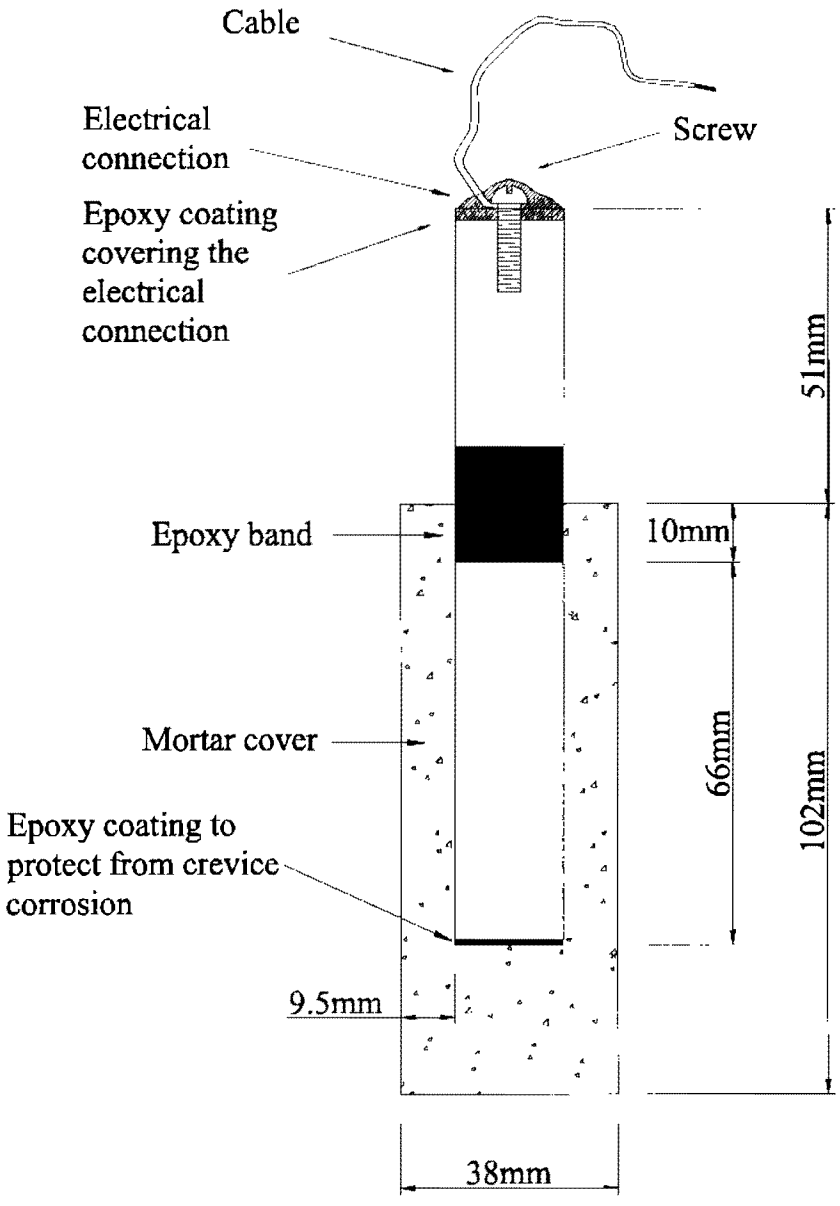

Figure 2.1 "Lollipop" specimen with mortar cover.

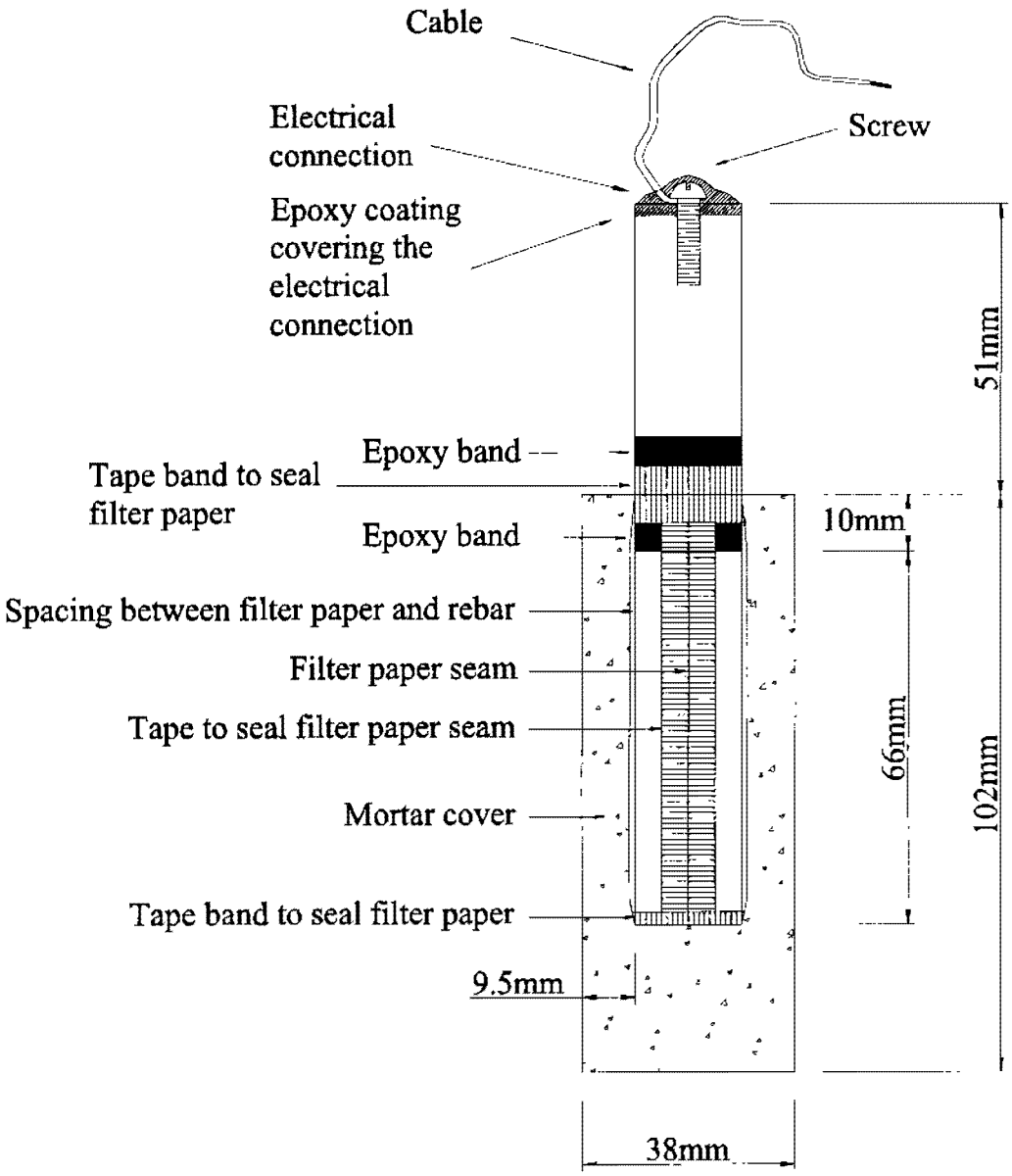

Figure 2.2 Lollipop specimen with filter paper wrapped and taped around the reinforcing bar.

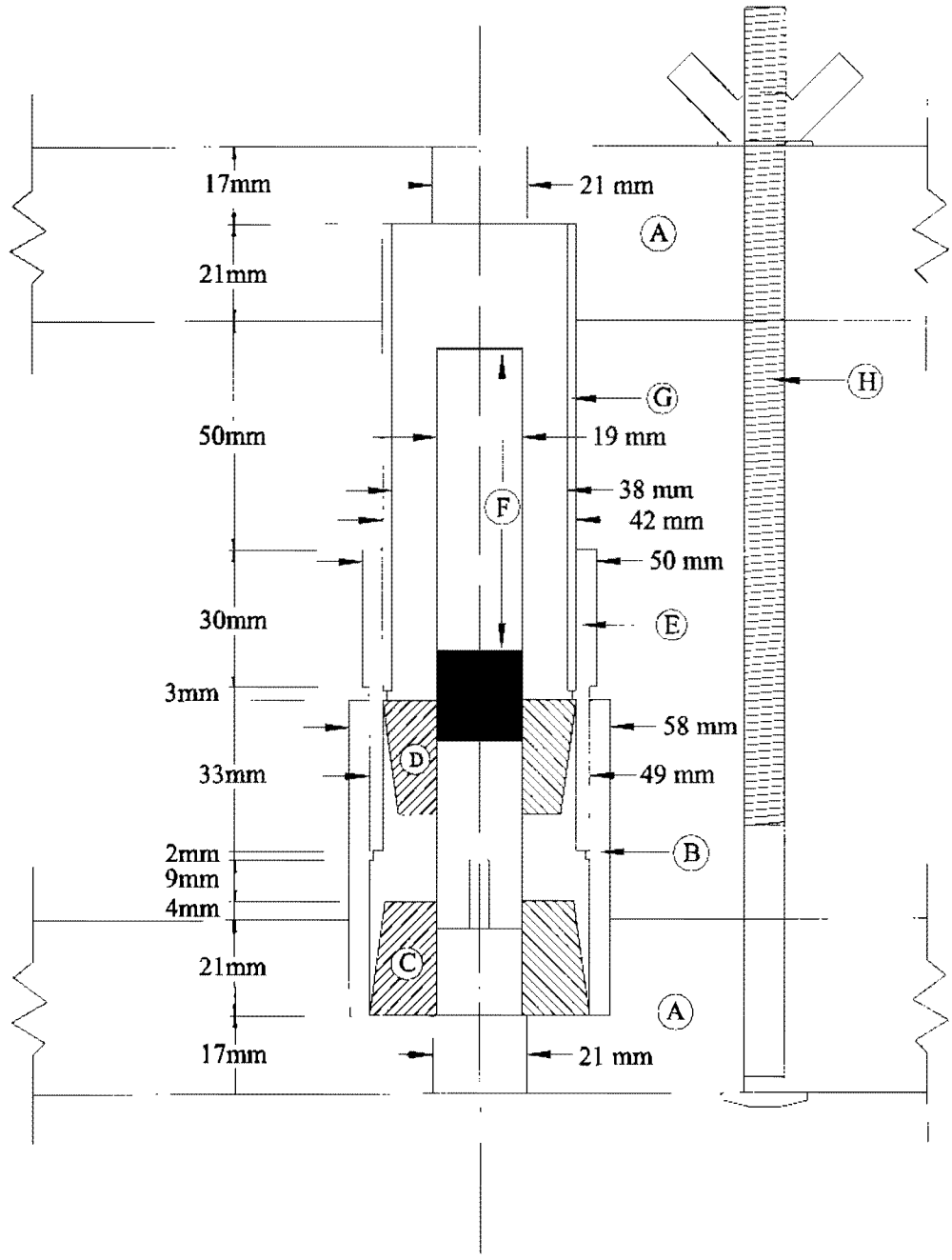

Figure 2.3 Mold for casting mortar specimens. Explanation of the respective parts is found in Table 2.1. Eight specimens were cast at one time.

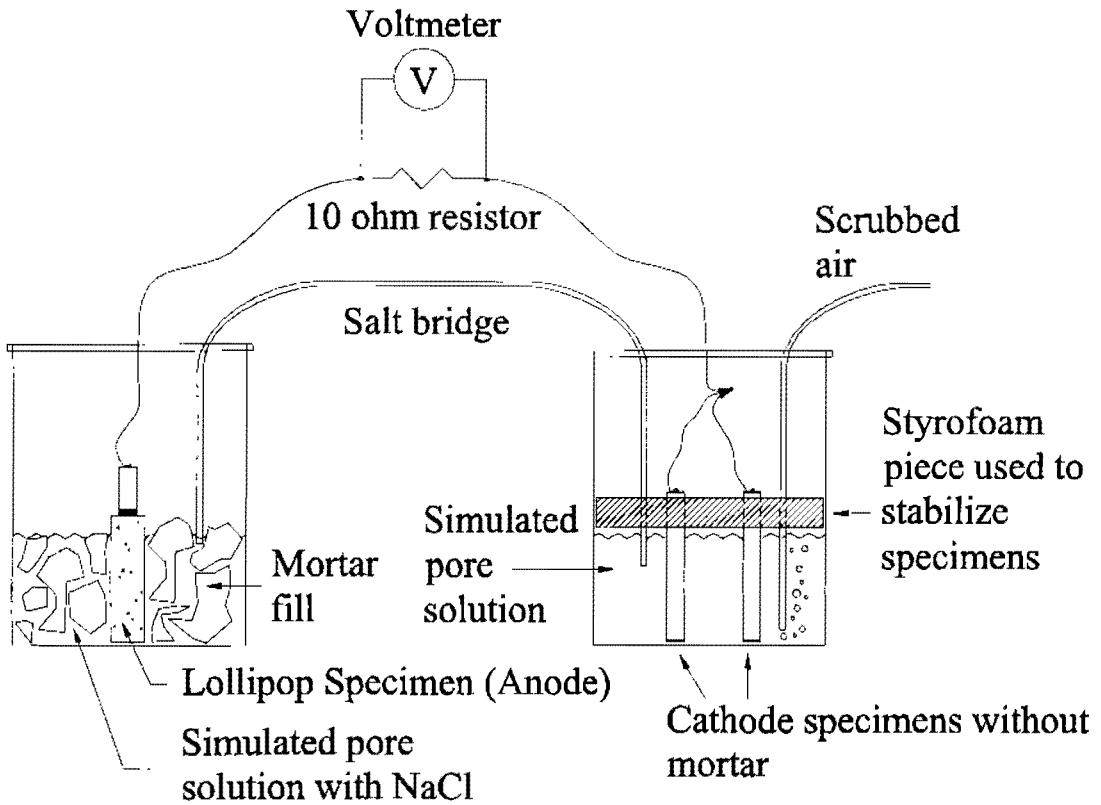

Figure 2.4 Test setup for macrocell test. Three lollipop specimens are submerged in pore solution with sodium chloride (anode solution) in a single container.

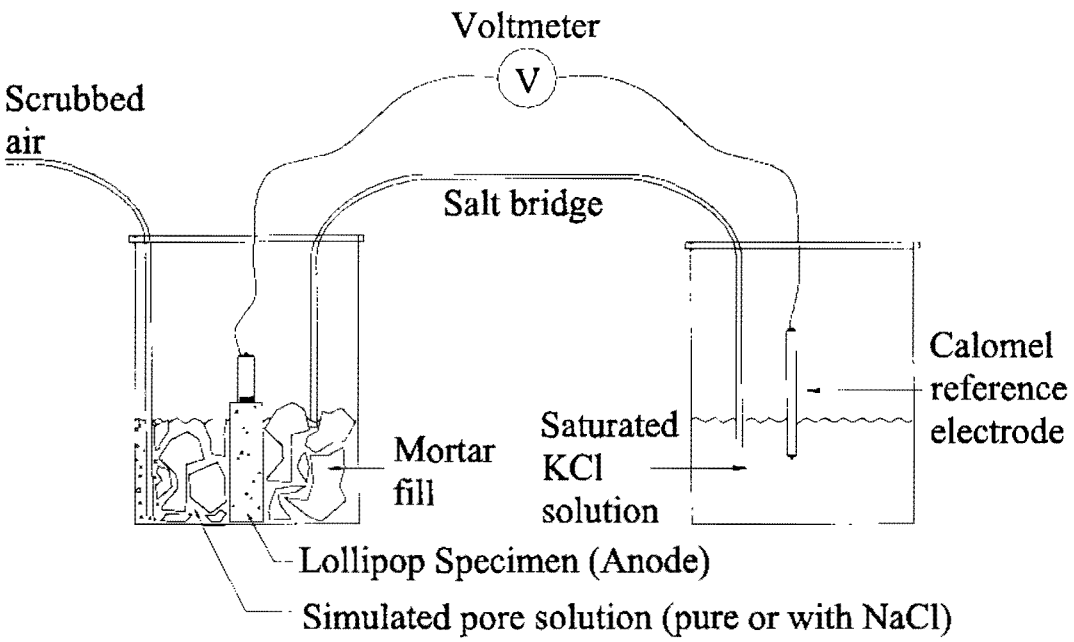

Figure 2.5 Test setup for corrosion potential test. Four lollipop specimens are submerged in the same container.

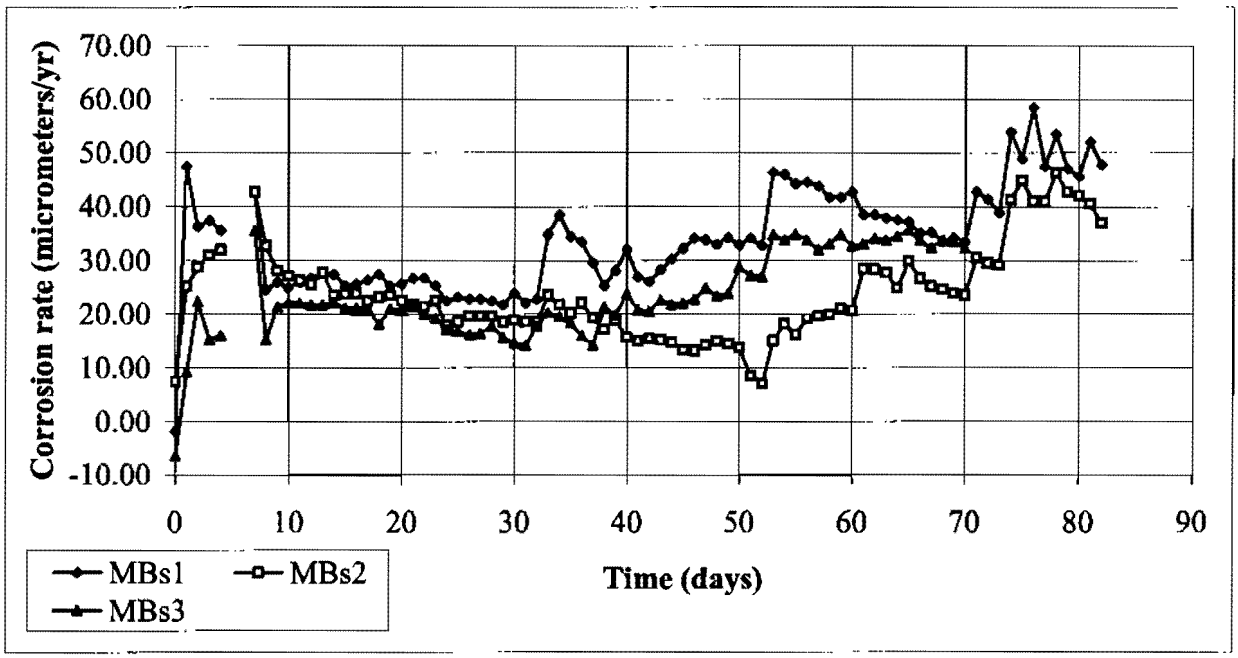

Figure 3.1 Macrocell test: Black steel No. 5 bars without mortar (all anodes submerged in same solution). Change of salt bridge on day 34 explains jump in corrosion rate. Salt bridges added on days 73 and 75.

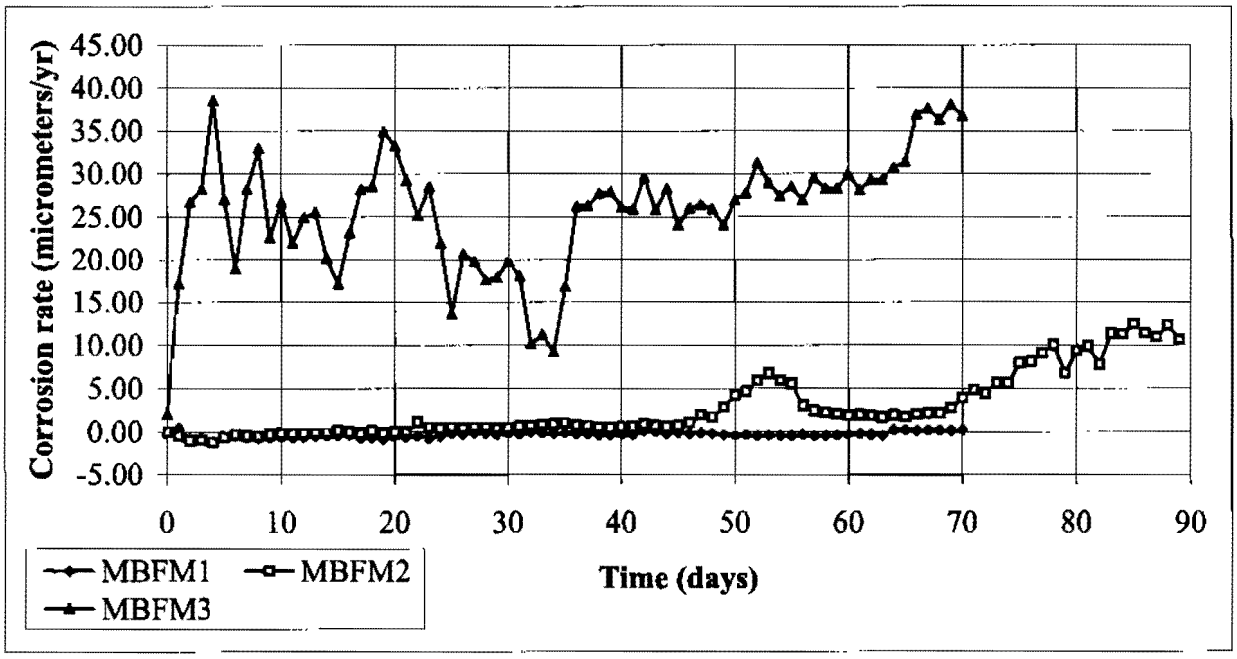

Figure 3.2 Macrocell test: Black steel No. 6 bars with mortar and one piece of filter paper (all anodes submerged in same solution). Specimen MBFM1 was moved to a separate container on day 64.

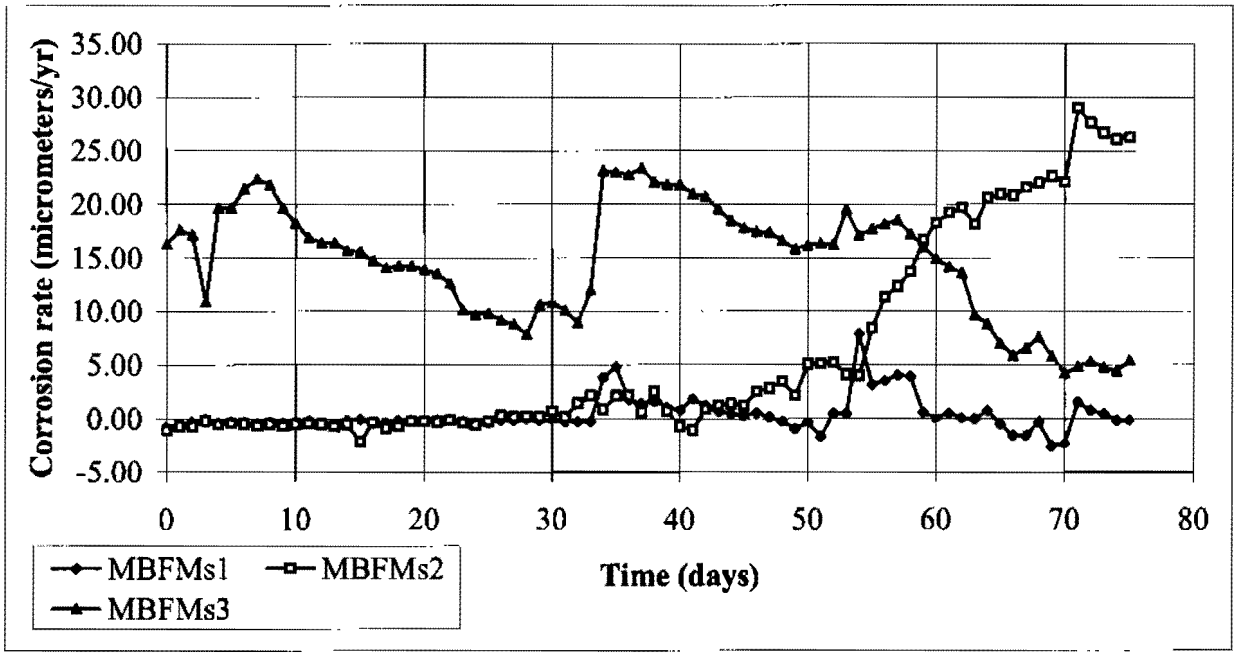

Figure 3.3 Macrocell test: Black steel No. 5 bars with mortar and one piece of filter paper (all anodes submerged in same solution). Specimen MBFMs1 was moved to a separate container on day 70.

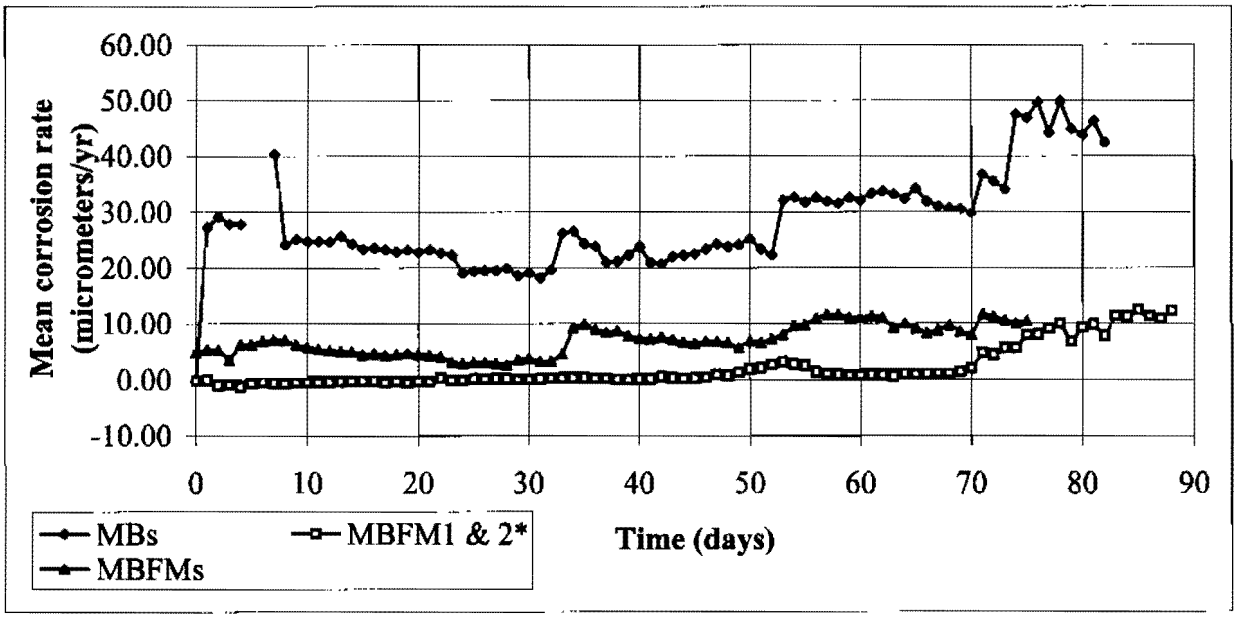

Figure 3.4 Macrocell tests: Mean corrosion rates for No. 5 bars without mortar (MBs) and No. 5 and No. 6 bars with mortar and one piece of filter paper (MBFMs and MBFM1 & 2, respectively). MBFM3 was excluded from the mean value calculation. * MBFM2 after day 70.

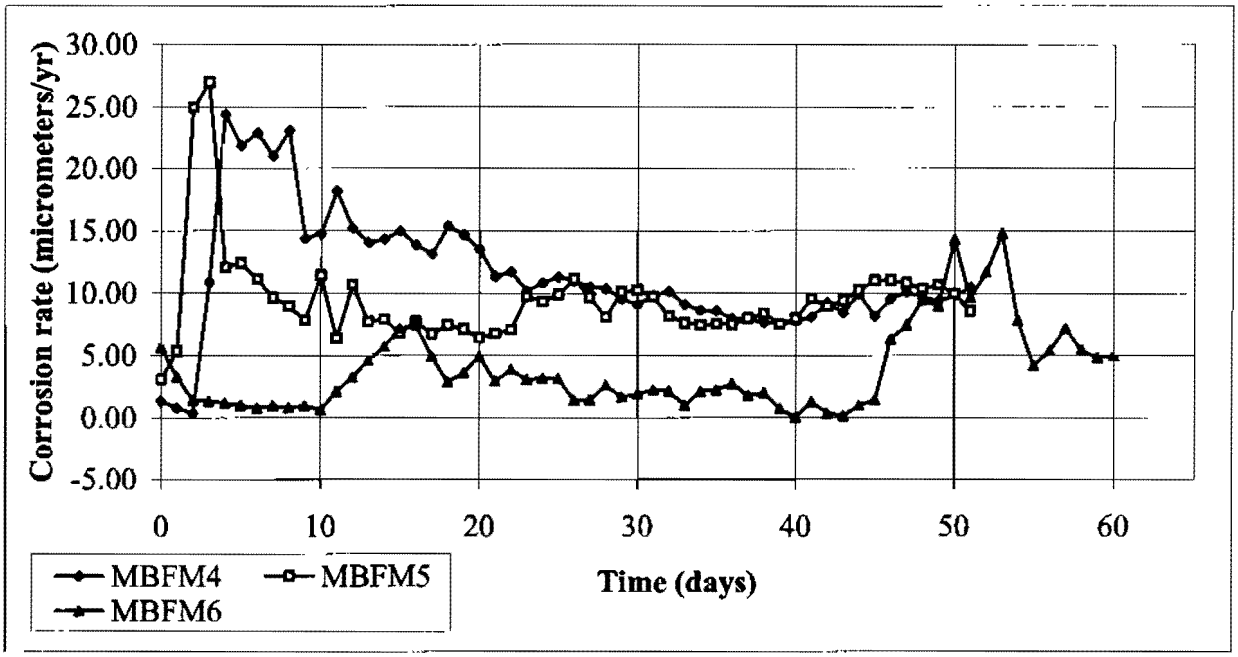

Figure 3.5 Macrocell test: Black steel No. 6 bars with mortar and two pieces of filter paper (all anodes submerged in same solution). MBFM6 moved to new solution on day 43.

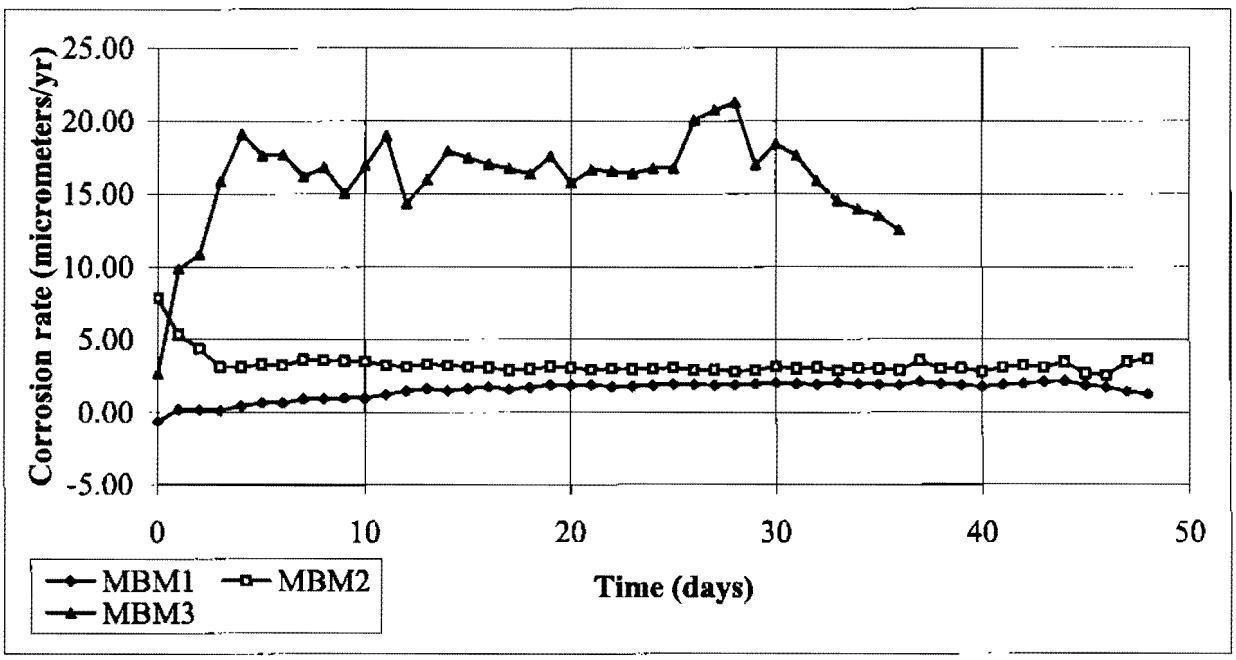

Figure 3.6 Macrocell test: Black steel No. 6 bars with mortar and no filter paper (all anodes submerged in same solution). MBM3 was discontinued due to unusually high corrosion rate.

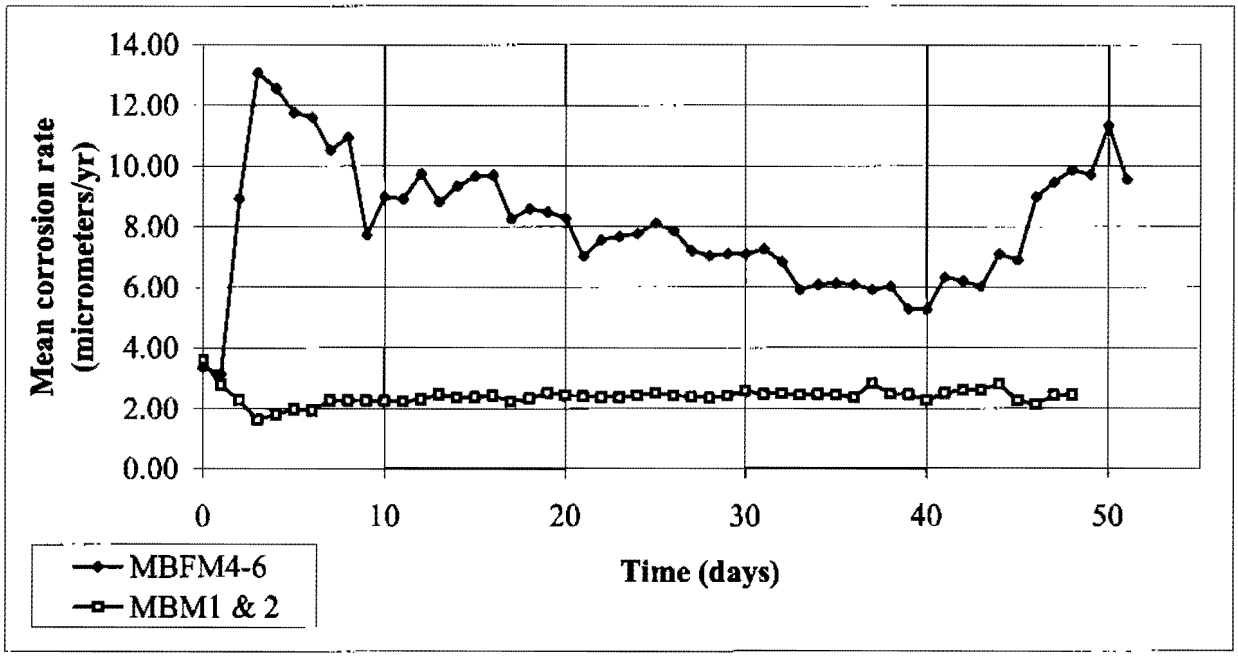

Figure 3.7 Macrocell tests: Mean corrosion rates for specimens with mortar and two pieces of filter paper (MBFM4-6) and specimens with mortar but without filter paper (MBM1 & 2). MBM3 was excluded from the calculation.

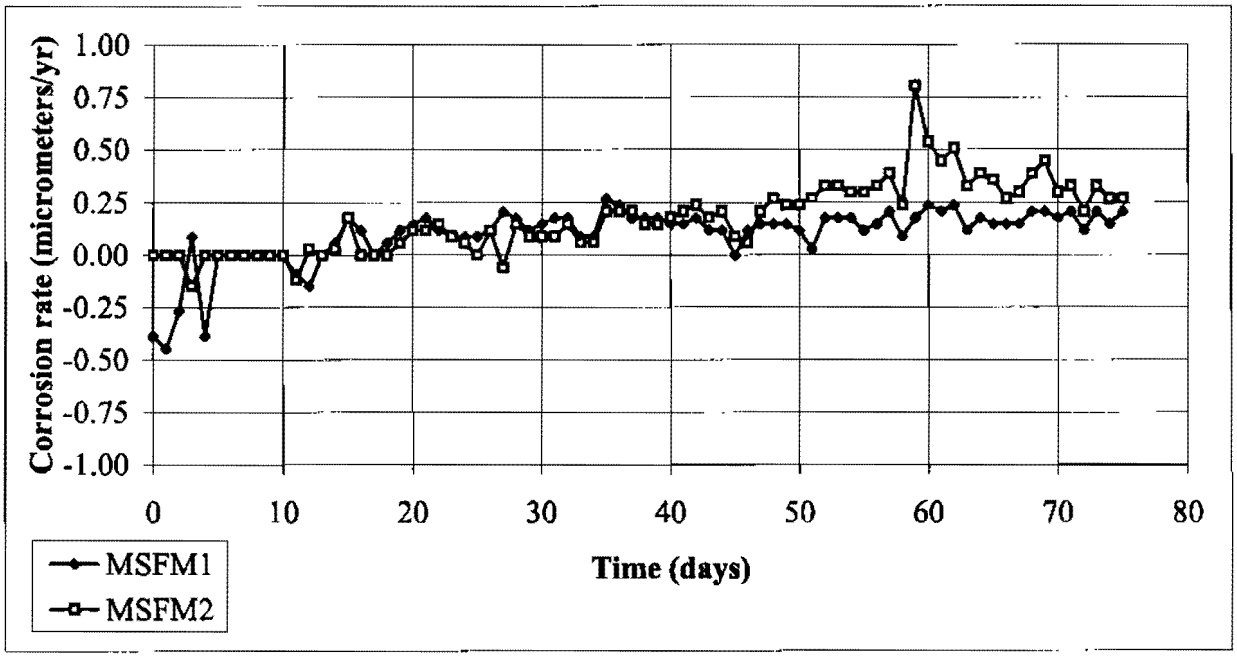

Figure 3.8 Macrocell test: Stainless steel clad No. 6 bars with mortar and one piece of filter paper (all anodes submerged in same solution).

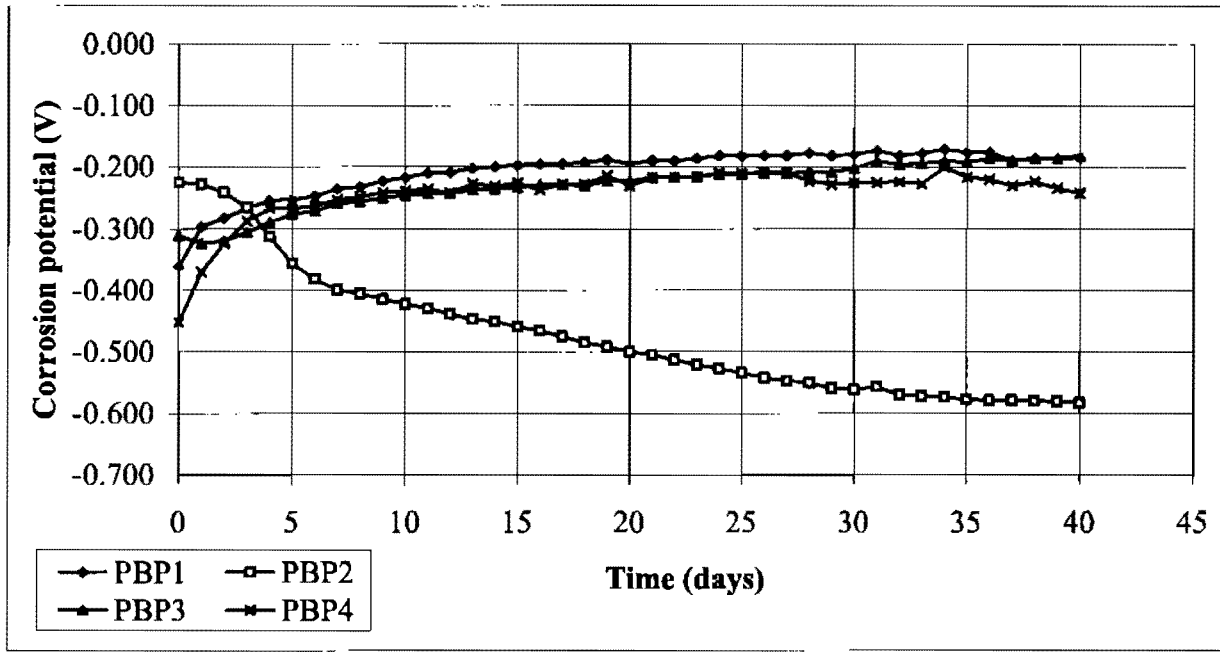

Figure 3.9 Corrosion potential test: Black steel No. 6 bars with mortar in simulated pore solution. PBP2 has epoxy coating on entire air-exposed part of the bar.

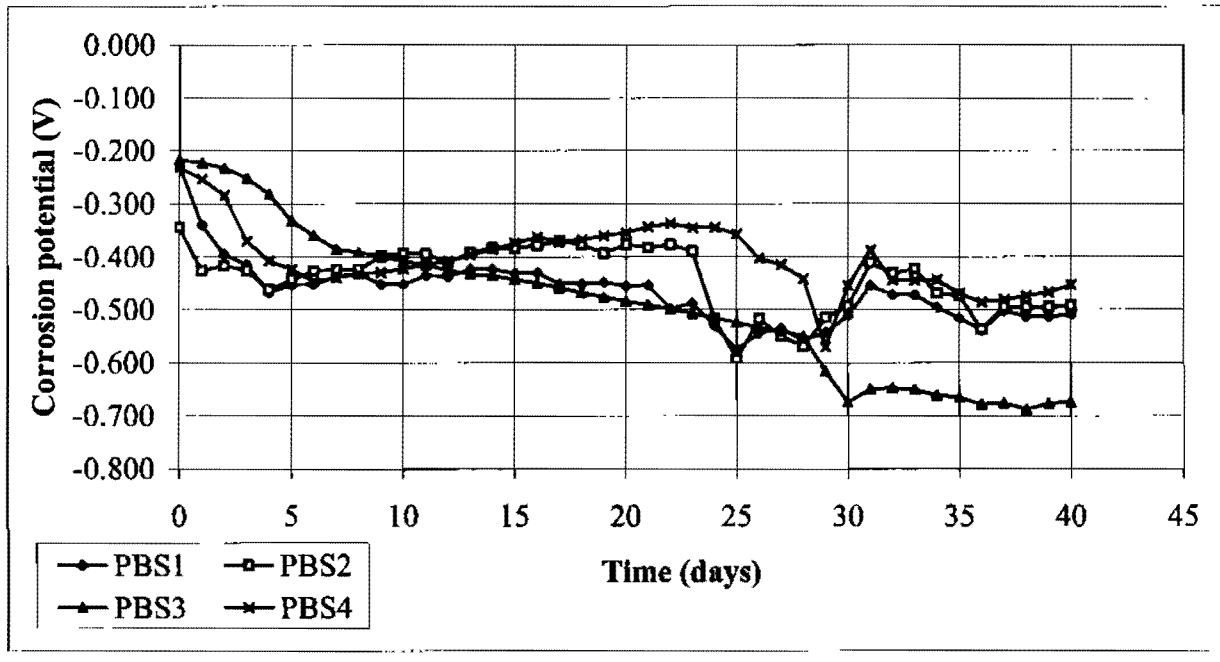

Figure 3.10 Corrosion potential test: Black steel No. 6 bars with mortar in pore solution with sodium chloride. PBS3 has epoxy on entire air-exposed part of the bar.

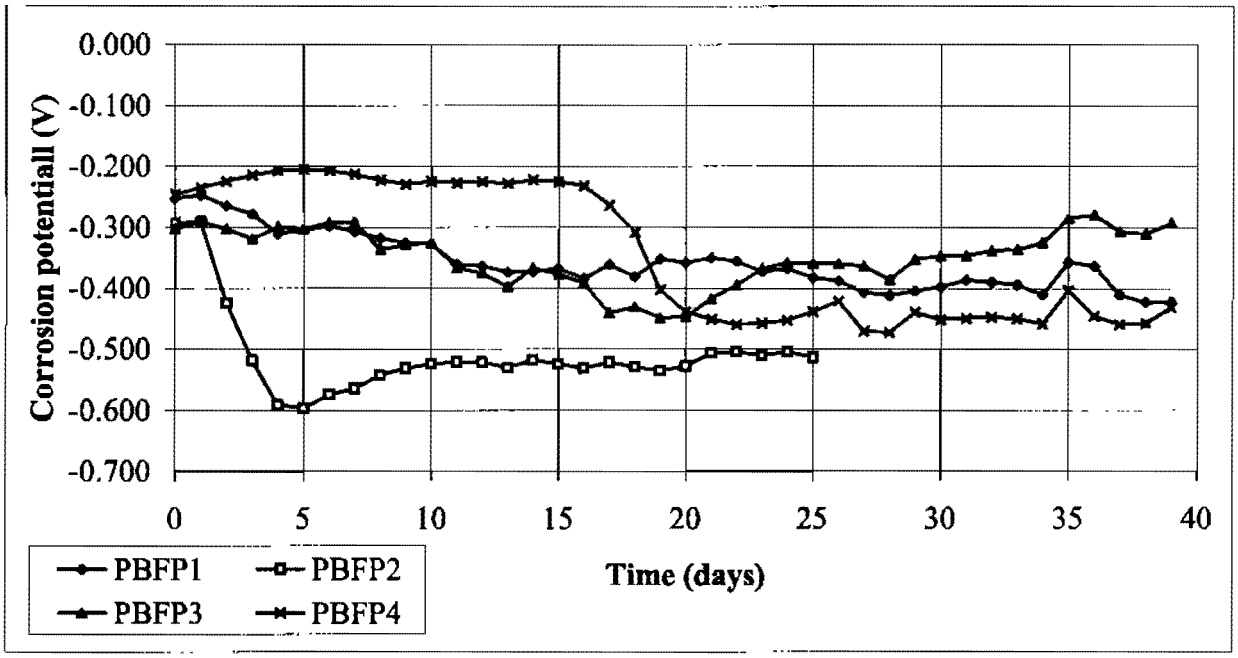

Figure 3.11 Corrosion potential test: Black steel No. 6 bars with mortar and two pieces of filter paper submerged in simulated pore solution.

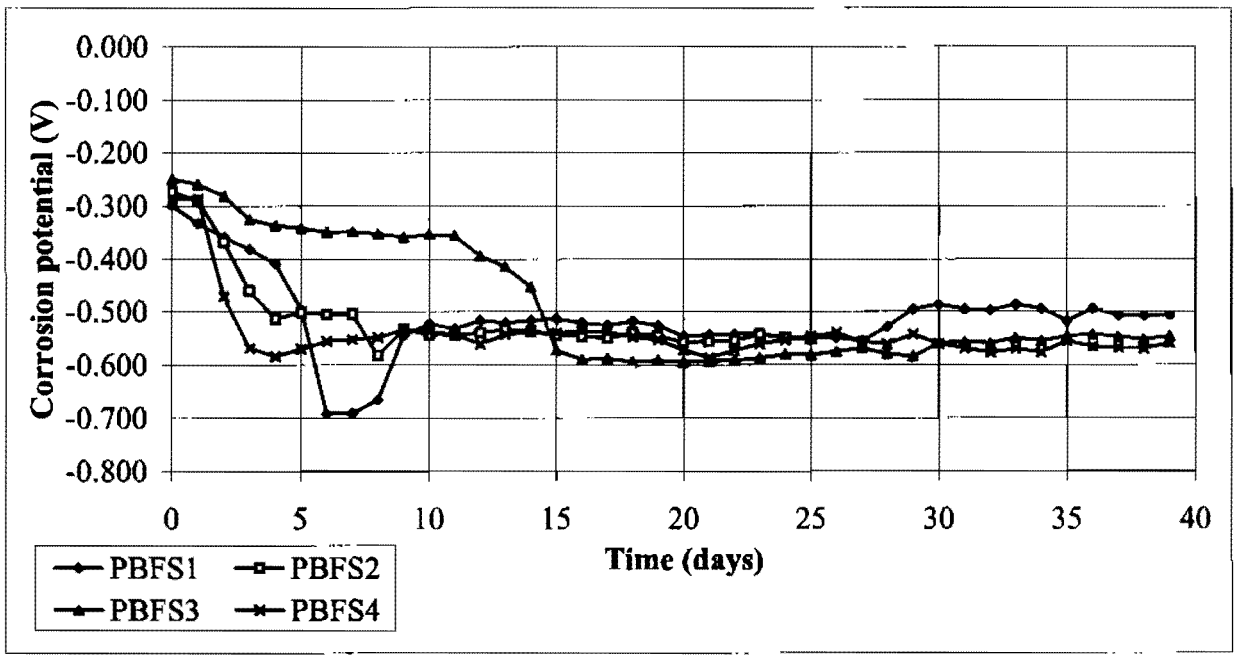

Figure 3.12 Corrosion potential test: Black steel No. 6 bars with mortar and two pieces of filter paper submerged in pore solution with sodium chloride.

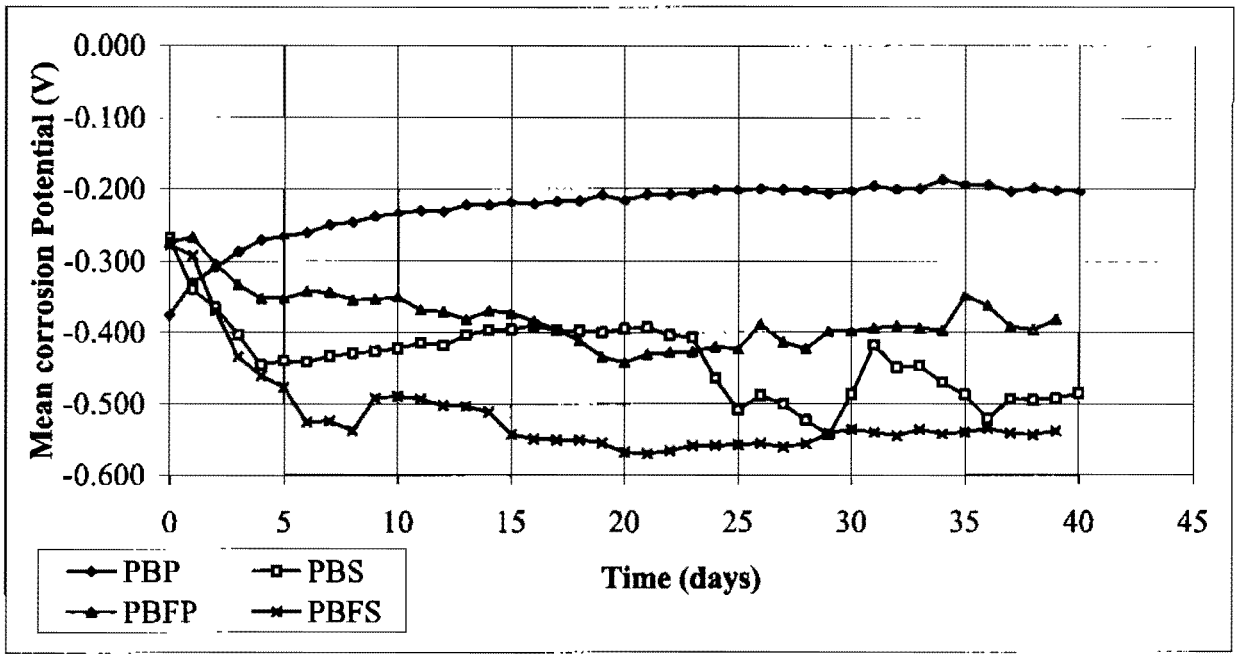

Figure 3.13 Corrosion potential tests: Mean corrosion rate for specimens without filter paper in pore solution (PBP) and pore solution with salt (PBS) and specimens with two pieces of filter paper in pore solution (PBFP) and in pore solution with salt (PBFS).

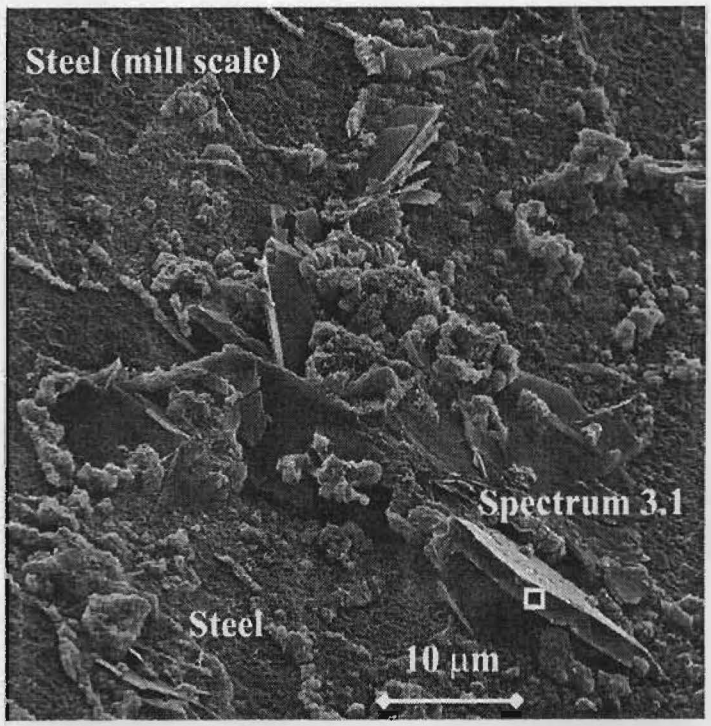

Figure 3.14 $Ca(OH)_2$ crystals on steel surface of specimen MBFM1 (Group 1: non-corroding, good adhesion). Spectrum 3.1 shows strong peaks for Ca and O. Magnification = 1550x (14 kV).

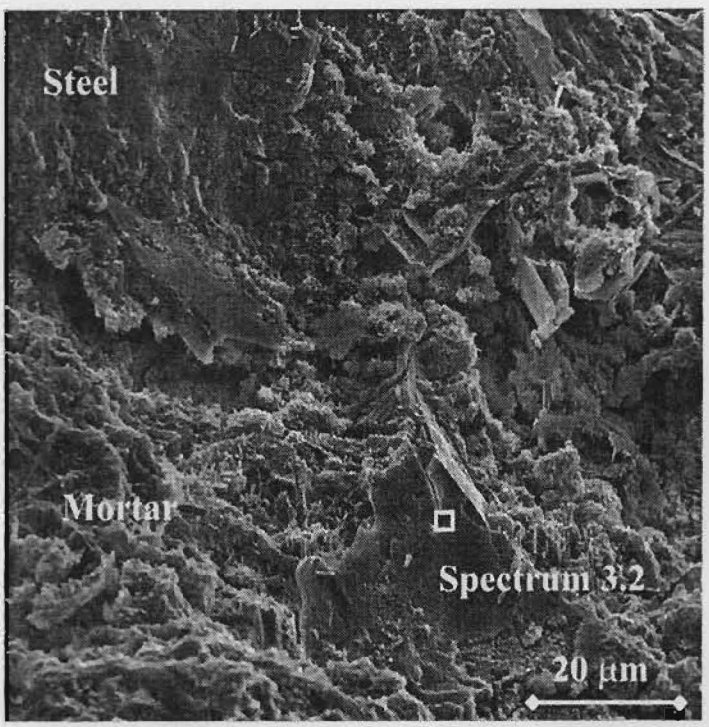

Figure 3.15 Micrograph showing steel surface of specimen MBM3 (Group 3: corroding, good adhesion) covered with cementitious material. The spectrum is taken from a $Ca(OH)_2$ crystal. Image at 845x (14 kV).

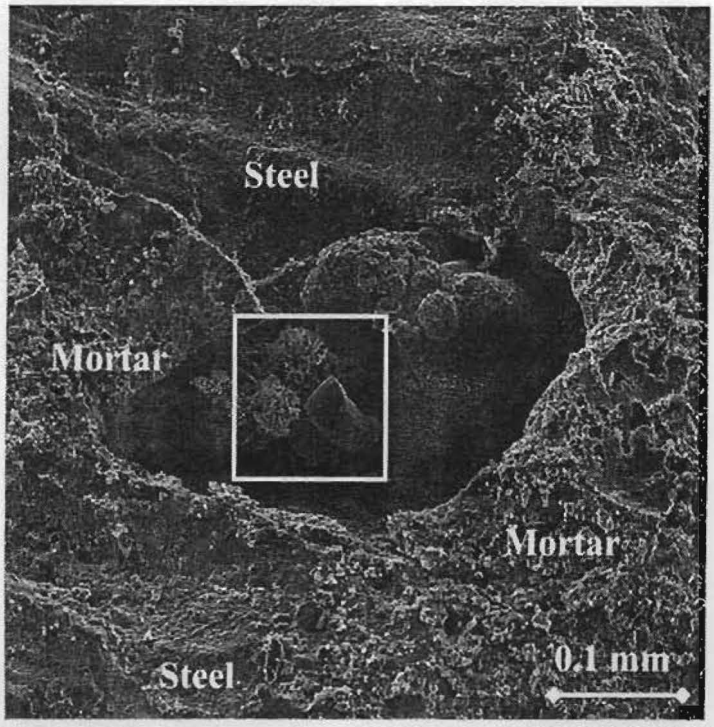

Figure 3.16 Corrosion products formed in void in mortar cover on specimen MBM3 (Group 3: corroding, good adhesion). Image taken at 150x (13 kV).

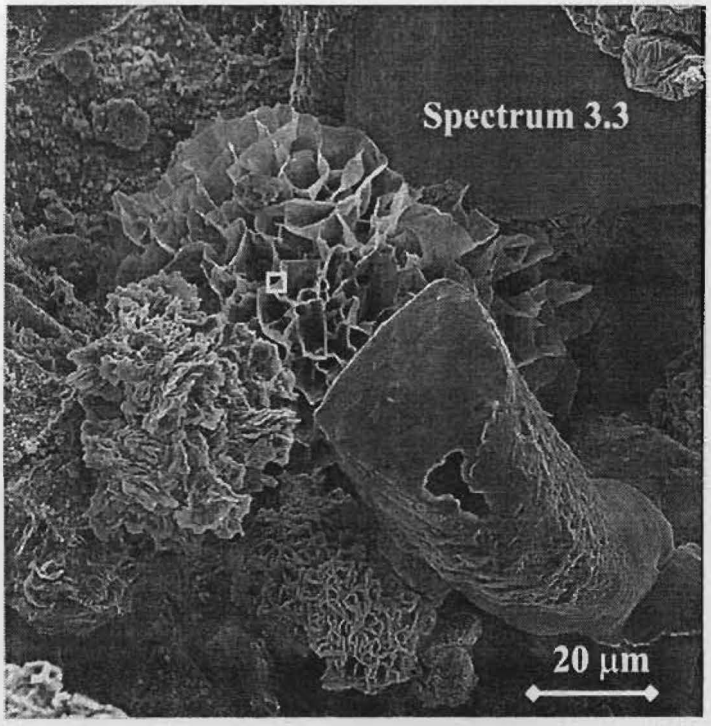

Figure 3.17 Zoom in on Figure 3.16 shows corrosion products of different morphologies. Micrograph recorded at 680x (10 kV).

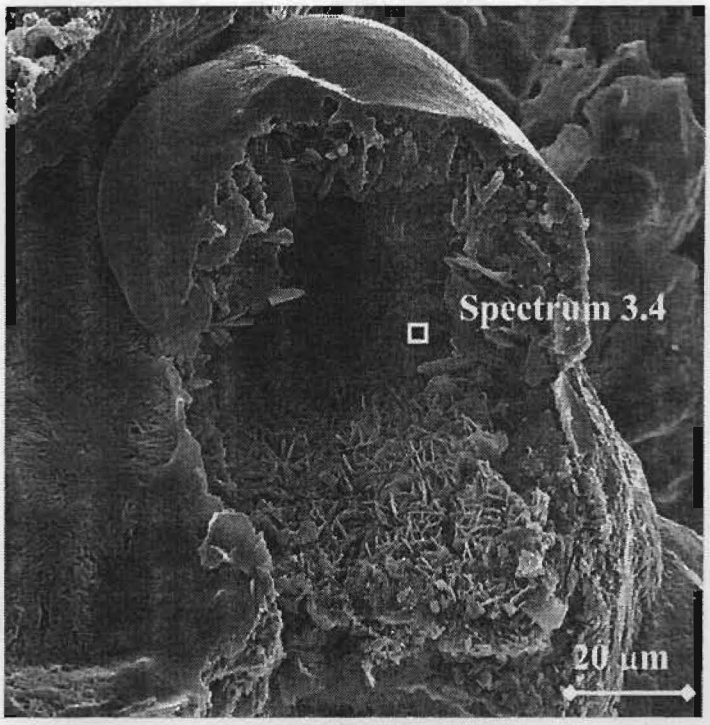

Figure 3.18 Corrosion products grown in a "pipe" on specimen MBFM5 (Group 4: corroding, poor adhesion). Image at 680x (20 kV).

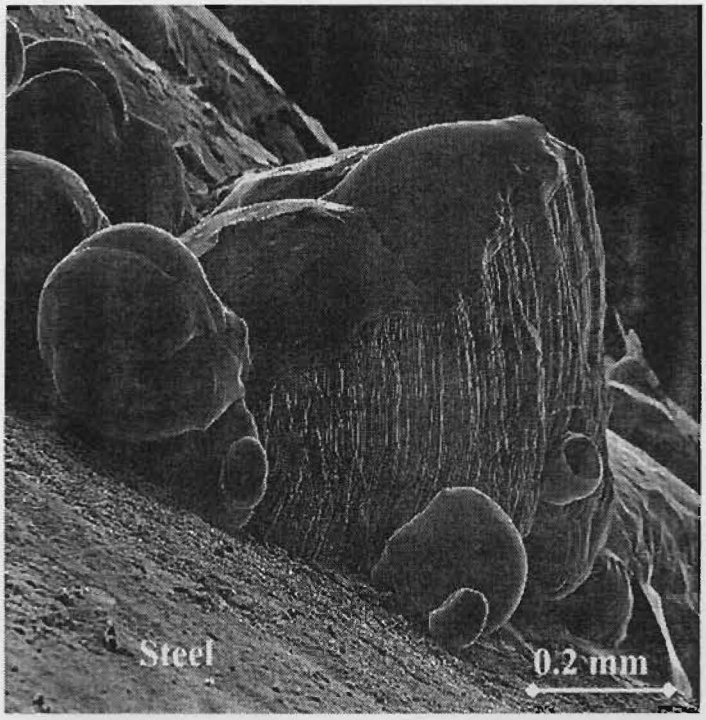

Figure 3.19 Corrosion products allowed growing on steel surface. Image taken at 81.5x (specimen MBFM5, 20 kV).

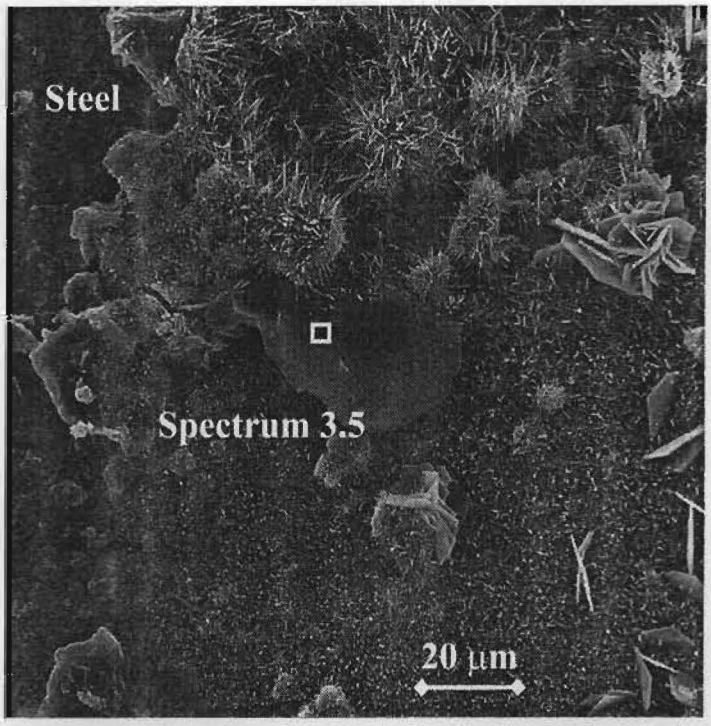

Figure 3.20 $Ca(OH)_2$ and products of cement hydration on the steel surface of specimen MBFM5. Small amounts of cementitious material have leaked through the filter paper and deposited on the steel surface. Image taken at 600x (20 kV).

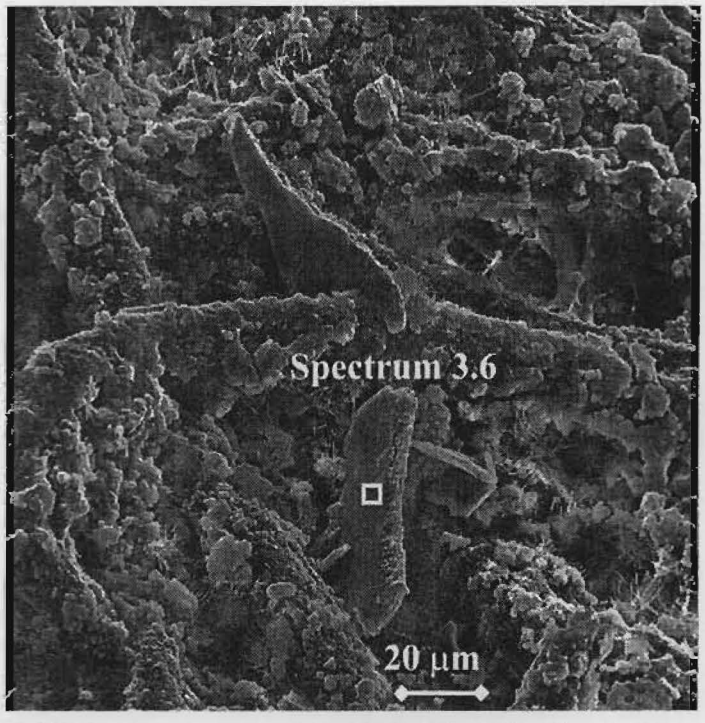

Figure 3.21 $Ca(OH)_2$ crystals grown on the inside of the inner filter paper on specimen MBFM5. Image at 462x (20 kV).

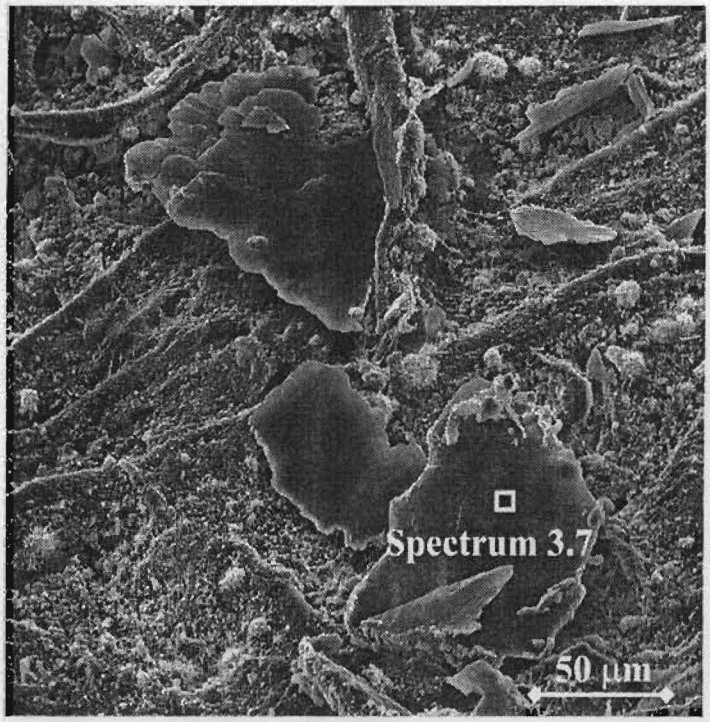

Figure 3.22 $Ca(OH)_2$ crystals formed on the inner surface of the outer filter paper of specimen MBFM5. Micrograph at 274x (20 kV).

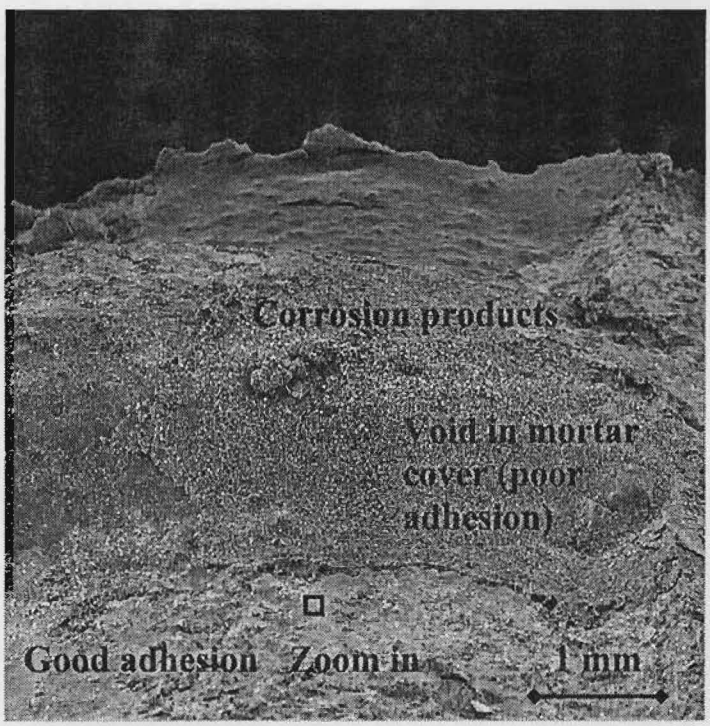

Figure 3.23 Image showing an area on specimen MBFMs1 that has both good and poor adhesion. Some poorly defined cementitious material has been deposited on the steel surface in the void. Image at 13.8x (12 kV)

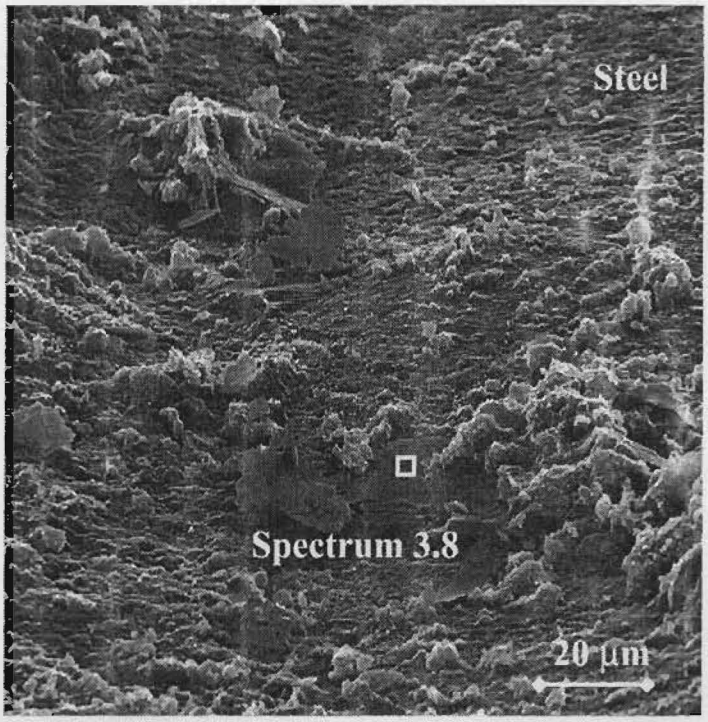

Figure 3.24 Zoom in on area as indicated in Figure 3.23 showing $Ca(OH)_2$ crystals on the steel surface. This area had good mortar adhesion. Micrograph taken at 625x (25 kV).

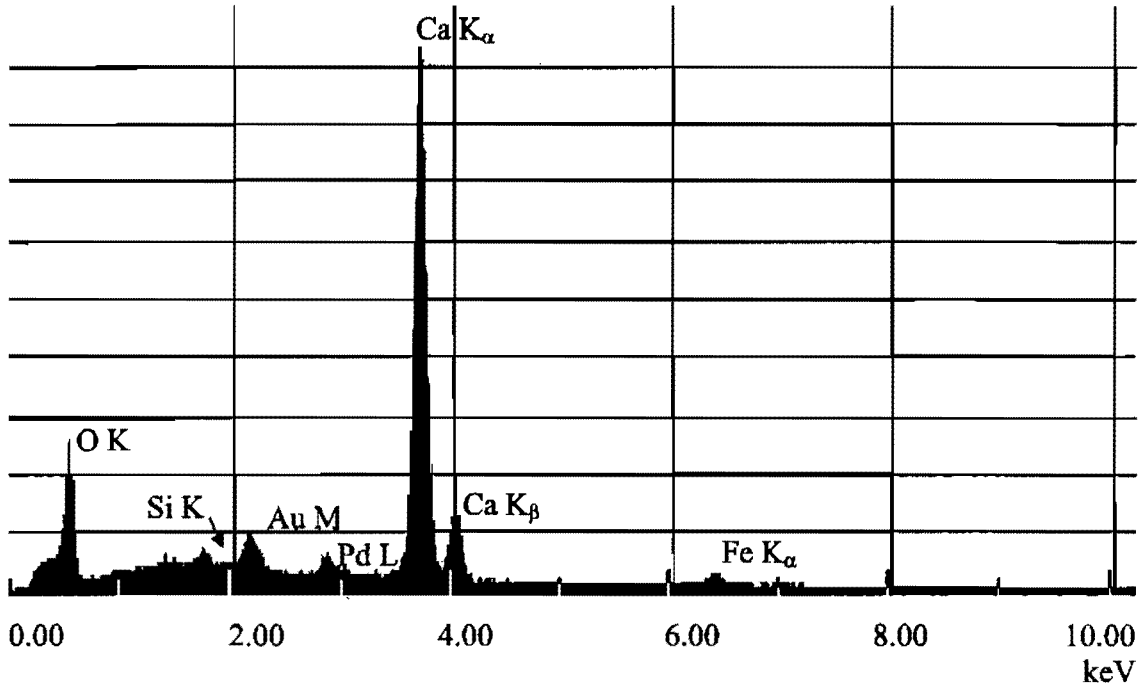

Spectrum 3.1 Spectrum showing large peaks for O and Ca and small peaks for Si and Fe on specimen MBFM1 (Figure 3.14). The specimen was coated with Au-Pd and the spectrum was recorded at 14 kV (live time = 253 sec.).

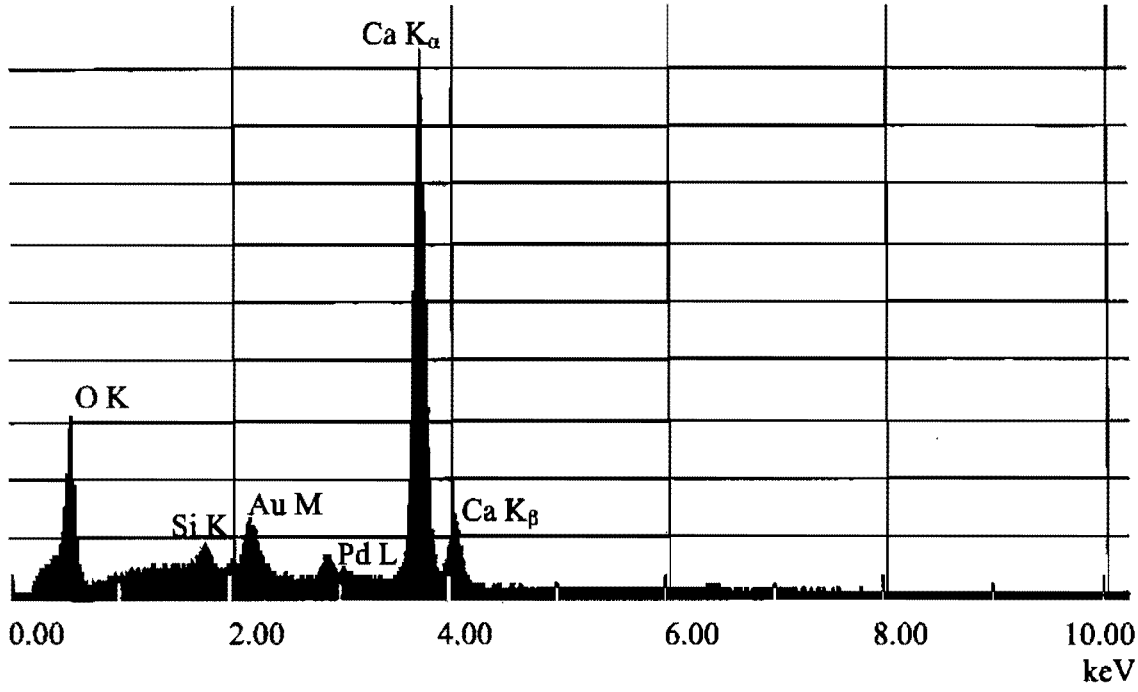

Spectrum 3.2 Large peaks for O and Ca and a small peak for Si from spectrum of calcium hydroxide crystals on specimen MBM3. The specimen was coated with Au-Pd. The spectrum was taken at 14 kV (155 sec. live time).

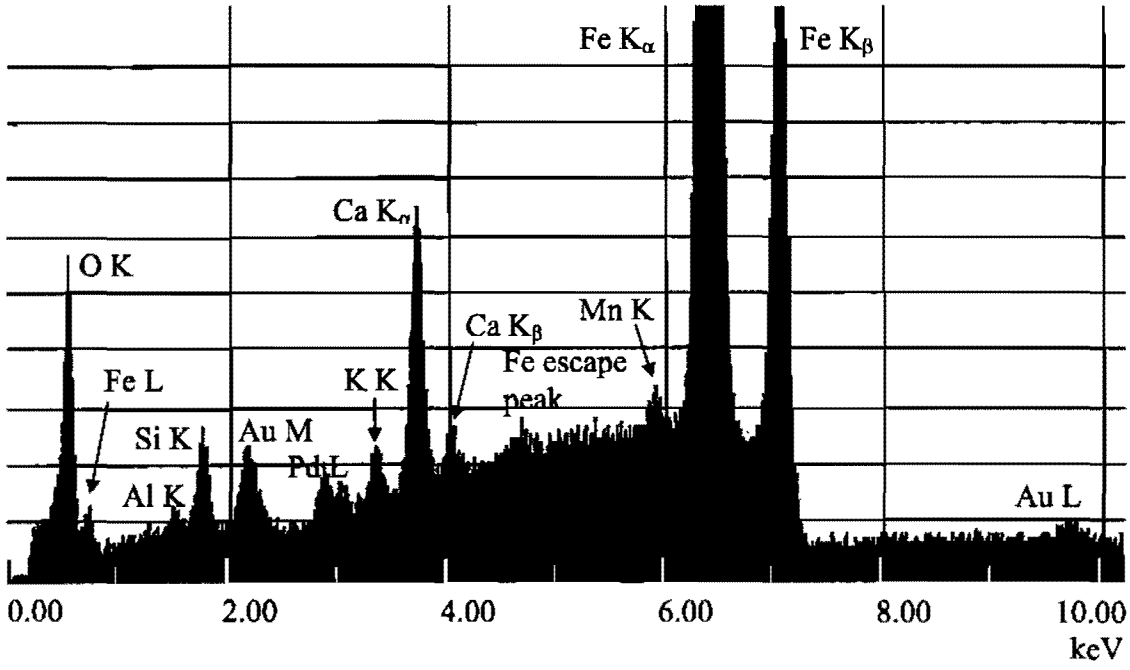

Spectrum 3.3 Spectrum from corrosion products shown in Figure 3.17 with strong peaks for O, Ca and Fe and smaller peaks for Al, Si, K and Mn. The specimen was coated with Au-Pd. Spectrum at 14 kV (live time =255 sec.)

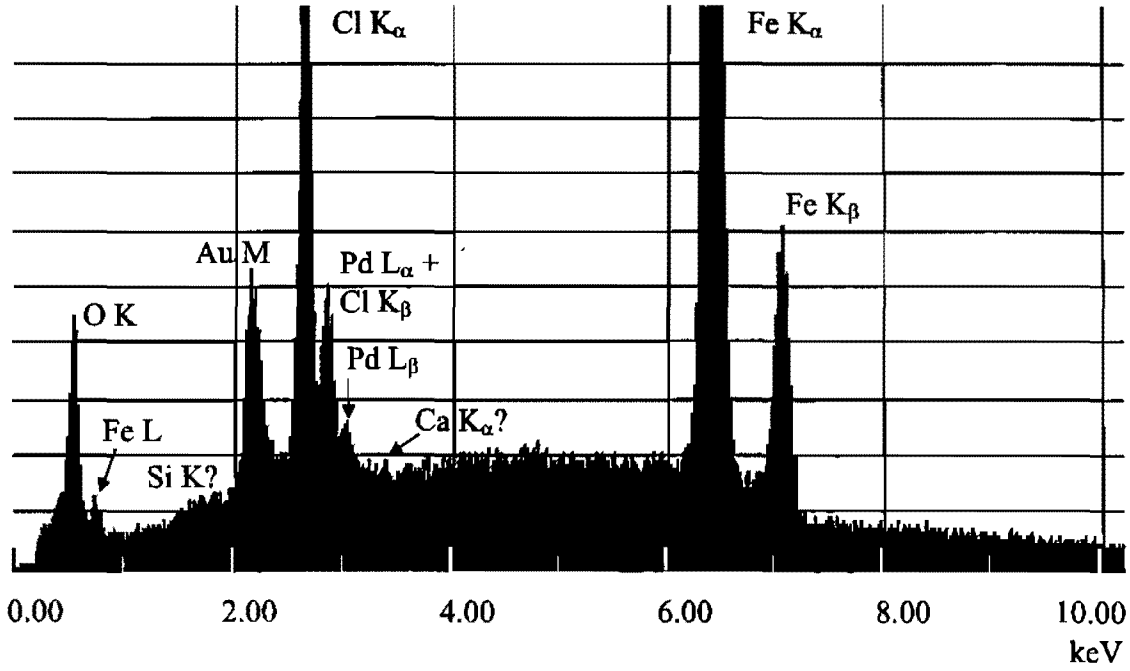

Spectrum 3.4 Spectrum from corrosion products shown in Figure 3.18 with strong peaks for O, Cl, and Fe with possible traces of Si and Ca. The specimen was coated with Au-Pd. Spectrum recorded at 12 kV (177 sec. live time).

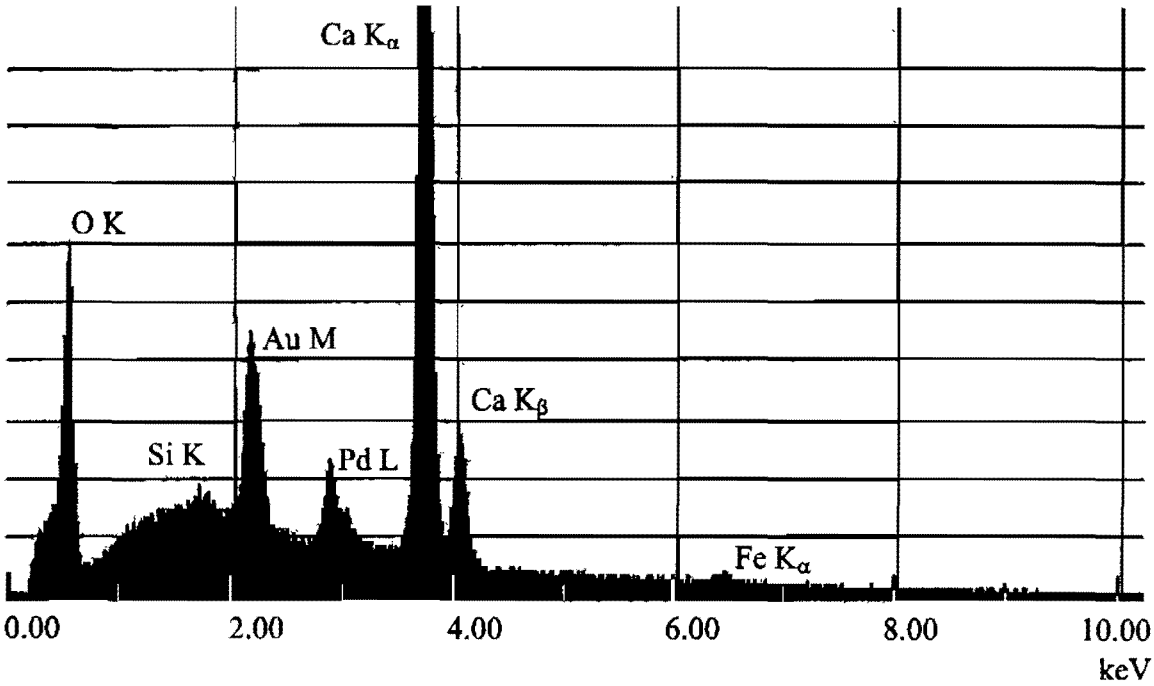

Spectrum 3.5 Calcium hydroxide on the steel surface of the Au-Pd coated specimen MBFM5 (Figure 3.20). Large peaks for O and Ca and very small peaks for Si and Fe. Spectrum taken at 10 kV (146 sec. live time)

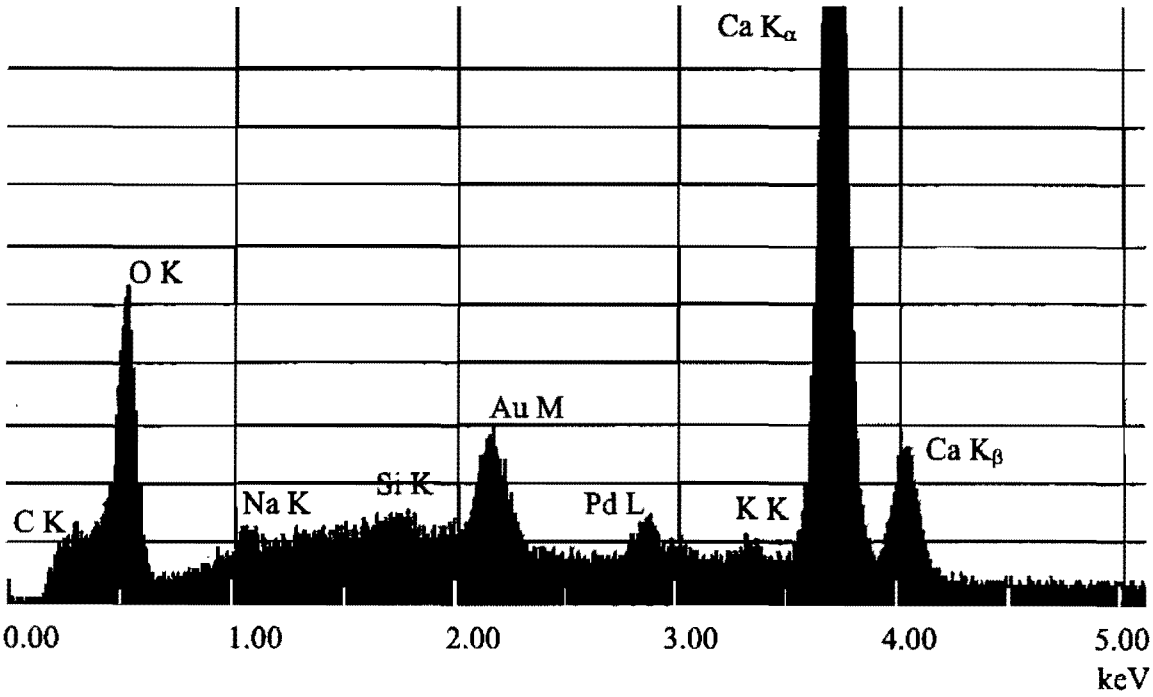

Spectrum 3.6 $Ca(OH)_2$ crystals grown on inner filter paper of the Au-Pd coated specimen MBFM5. The spectrum shows large peaks for O and Ca and small peaks for C, Na, Si and K. Spectrum taken at 10 kV (221 sec.).

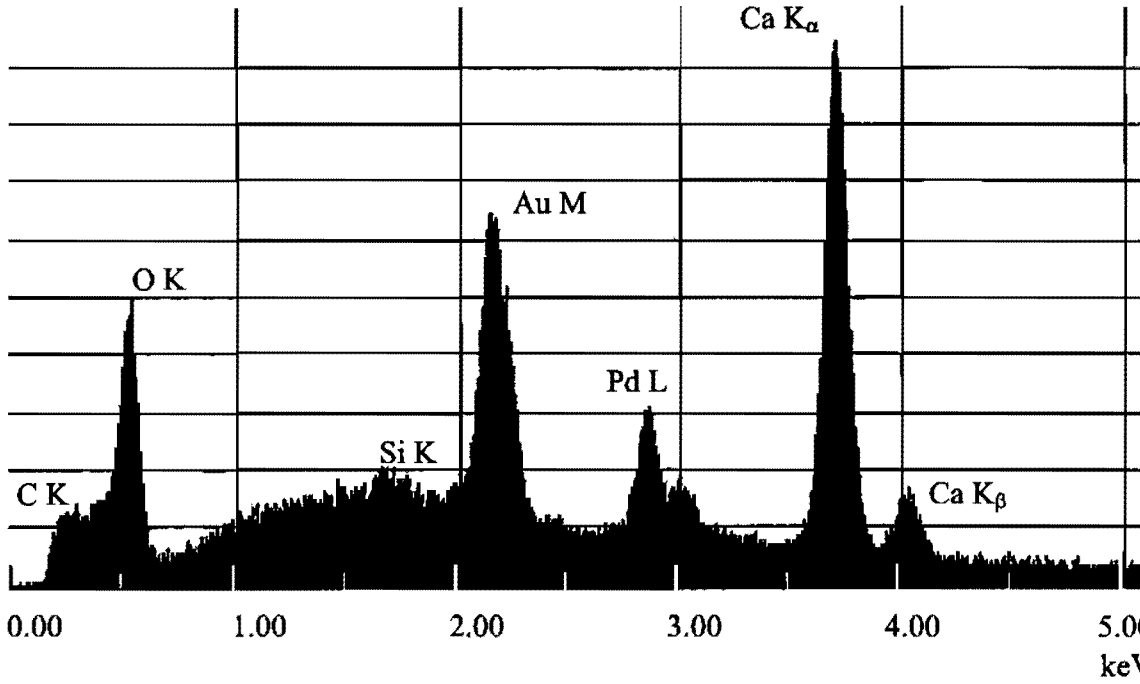

Spectrum 3.7 $Ca(OH)_2$ crystals grown on the outer filter paper of the Au-Pd coated specimen MBFM5. Large peaks for O and Ca are shown as well as small peaks for C and Si. Spectrum recorded at 8 kV (338 sec. live time).

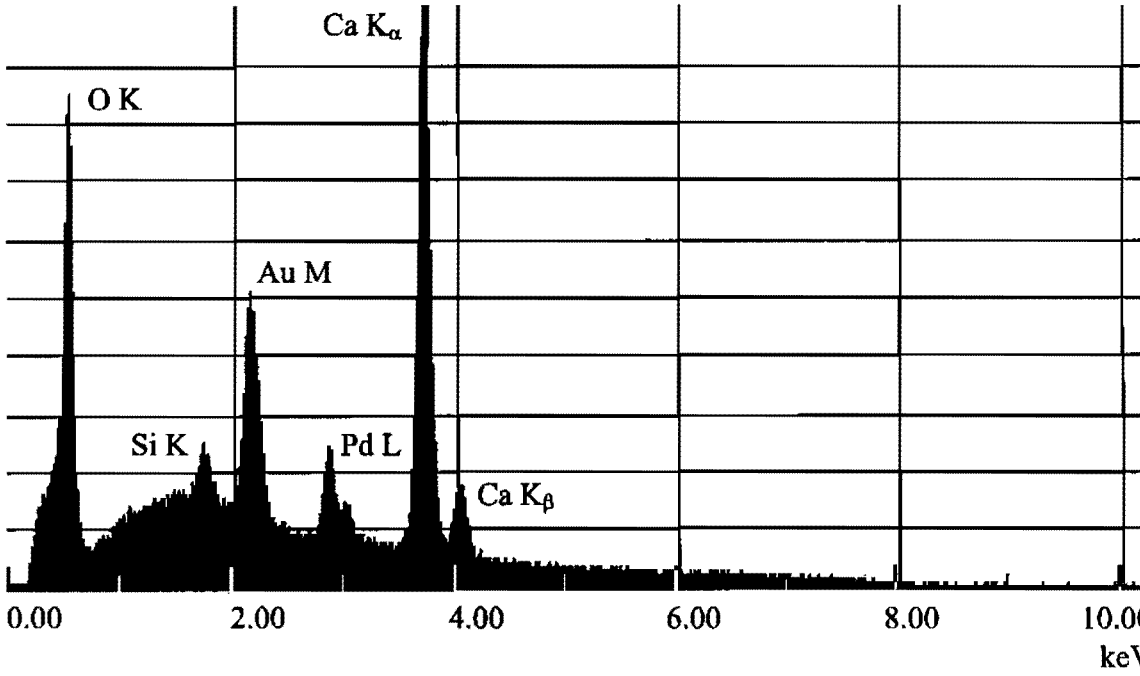

Spectrum 3.8 Spectrum of the Au-Pd coated specimen MBFMs1 showing large peaks for O and Ca and a small peak for Si. Spectrum recorded at 8 kV (194 sec. live time).